Thiosugar naphthalene diimide conjugates: G-quadruplex ligands with antiparasitic and anticancer activity

Efres Belmonte-Reche, Alessandra Benassi, Pablo Peñalver, Anne Cucchiarini, Aurore Guédin, Jean Louis Mergny, Frèdèric Rosu, Valerie Gabelica, Mauro Freccero, Filippo Doria, et al.

European Journal of Medicinal Chemistry 232 (2022) 114183

Contents lists available at ScienceDirect

European Journal of Medicinal Chemistry

journal homepage: http://www.elsevier.com/locate/ejmech

Thiosugar naphthalene diimide conjugates: G-quadruplex ligands with antiparasitic and anticancer activity

Efres Belmonte-Reche [a, 1], Alessandra Benassi [b, 1], Pablo Peñalver [a, 1], Anne Cucchiarini [c], Aurore Guédin [d], Jean Louis Mergny [c], Frèdèric Rosu [e], Valerie Gabelica [f], Mauro Freccero [b], Filippo Doria [b, **], Juan Carlos Morales [a, *]

[a] Department of Biochemistry and Molecular Pharmacology, Instituto de Parasitología y Biomedicina López Neyra, CSIC, PTS Granada, Avda. del Conocimiento, 17, Armilla, 18016, Granada, Spain
[b] Università di Pavia, Dipartimento di Chimica, Viale Taramelli 10, 27100, Pavia, Italy
[c] Laboratoire d'optique et Biosciences, Ecole Polytechnique, Inserm U1182, CNRS UMR7645, Institut Polytechnique de Paris, Palaiseau, France
[d] Université de Bordeaux, IECB, France
[e] Institut Européen de Chimie et Biologie, Université de Bordeaux, CNRS & Inserm (IECB, UMS3033, US001), 2 rue Robert Escarpit, 33607, Pessac, France
[f] Université de Bordeaux, CNRS, INSERM, ARNA, UMR 5320, U1212, IECB, F-33600 Pessac, France

ARTICLE INFO

Article history:
Received 29 November 2021
Received in revised form
27 January 2022
Accepted 3 February 2022
Available online 7 February 2022

Keywords:
DNA
G-quadruplex
Ligand
Conjugate
Carbohydrate
Anticancer
Antiparasitic

ABSTRACT

Glycosyl conjugation to drugs is a strategy being used to take advantage of glucose transporters (GLUT) overexpression in cancer cells in comparison with non-cancerous cells. Its extension to the conjugation of drugs to thiosugars tries to exploit their higher biostability when compared to *O*-glycosides. Here, we have synthesized a series of thiosugar naphthalene diimide conjugates as G-quadruplex ligands and have explored modifications of the amino sidechain comparing dimethyl amino and morpholino groups. Then, we studied their antiproliferative activity in colon cancer cells, and their antiparasitic activity in *T. brucei* and *L. major* parasites, together with their ability to bind quadruplexes and their cellular uptake and location. We observed higher toxicity for the sugar-NDI-NMe_2 derivatives than for the sugar-NDI-morph compounds, both in mammalian cells and in parasites. Our experiments indicate that a less efficient binding to quadruplexes and a worse cellular uptake of the carb-NDI-morph derivatives could be the reasons for these differences. We found small variations in cytotoxicity between *O*-carb-NDIs and *S*-carb-NDIs, except against non-cancerous human fibroblasts MRC-5, where thiosugar-NDIs tend to be less toxic. This leads to a notable selectivity for β-thiomaltosyl-NDI-NMe_2 **12** (9.8 fold), with an IC50 of 0.3 μM against HT-29 cells. Finally, the antiparasitic activity observed for the carb-NDI-NMe_2 derivatives against *T. brucei* was in the nanomolar range with a good selectivity index in the range of 30- to 69- fold.

1. Introduction

G-quadruplexes (G4) are nucleic acids secondary structures formed within guanine-rich sequences where the basic motif are guanine tetrads linked through Hoogsteen hydrogen bonds and stacked on top of each other. G4's are located in key regions of the genome such as in promoters, enhancers, and telomeres, playing important roles in cellular and genetic processes [1,2]. In the last decade, they have emerged as interesting targets for cancer [3–5], neurological pathologies [6,7], as well as for viral [8] and parasitic infections [9,10].

A wide variety of small molecule ligands have been reported to bind G-quadruplexes [11,12], but only a few based on naphthalene diimide [13], quinazoline [14], quinoxaline [15], among other aromatic scaffolds, have shown efficacy as anticancer agents in animal models. Of those, only Quarfloxin (CX-3543) [16], APTO-253 [17,18], CX-5461 [19], and recently pyrvinium pamoate [20], have managed to enter clinical trials for the treatment of different types of tumors.

Our research groups have described carbohydrate naphthtalene diimide conjugates (carb-NDIs) as potential anticancer [21] and antiparasitic agents [10,22]. Several mono- and disaccharide-NDIs resulted in submicromolar IC50 values against HT-29, MCF-7 and

* Corresponding author.
** Corresponding author.
E-mail addresses: filippo.doria@unipv.it (F. Doria), jcmorales@ipb.csic.es (J.C. Morales).
[1] E.B.R., A.B. and P.P. contributed equally.

https://doi.org/10.1016/j.ejmech.2022.114183

HeLa cancerous cells, with 1.4- to 5.4-fold less toxicity against non-cancerous MRC-5 cells. The activity of these carb-NDIs against *Trypanosoma brucei*, the parasite causing sleeping sickness, showed IC50 values in the nanomolar range with 40- to 80-fold selectivity when compared to MRC-5 human cells. The carbohydrate conjugation to potential chemotherapy drugs tries to take advantage of the Warburg effect, since rapidly proliferating cancer cells have a different energy metabolism than that of healthy cells. This process is characterized by the sole use of the glycolytic pathway for the partial catabolism of carbohydrates compared to the complete route through the posterior metabolism of pyruvate in the citric acid cycle. Although this provides benefits for the survival of cancer cells, it ultimately yields less ATP and hence transmembrane glucose transporters (GLUTs) are overexpressed in compensation to ensure that sufficient glucose is internalized to ensure its growth. Thus, sugar conjugation becomes an attractive system for targeted drug delivery directly to cancer cells. In fact, this approach is becoming popular for all types of drugs [23], such as metallodrugs [24–26], peptides [27], oligonucleotides [28] or natural products [29], and glufosfamide, a glucose-ifosfamide conjugate, is in clinical trials Phase III for pancreatic cancer.

In our first work on carb-NDIs [21] we showed that the higher selectivity of the carbohydrate-NDIs for tumoral cells was due to its preferential uptake through the overexpressed glucose transporters, especially through GLUT 1 and GLUT 4. This has been recently confirmed in a collaborative work where a lactose-C-NDI derivative (Fig. S1) showed a 4-fold greater entrance into tumoral cells (SW480) in relation to non-tumoral ones as quantified by confocal fluorescence microscopy [30]. At the same time, lactose-C-NDI showed selective inhibition of cell growth by high-affinity binding to G-quadruplexes in ribosomal DNA, hindering RNA polymerase I (Pol I) elongation. Thus, lactose-C-NDI induced inhibition of Pol I transcription, nucleolus disruption, degradation of the proteasome-dependent Pol I catalytic subunit A and finally, autophagy.

Conjugation of thioglycosides to drugs instead of *O*-glycosides has also been used due to their higher biochemical stability to glycosidases [31,32], in order to potentially improve their bioavailability under physiological conditions. Moreover, thiosugars may bring differences on GLUT binding which could be interesting to explore with NDI conjugates. In fact, this approach has already been used on thiosugar nanoparticle conjugates [33], thiosugar peptides [34], thiosugar dendrimers [35] and also on thiosugar drugs, such as, auranofin [36], a drug to treat rheumatoid arthritis or GOPI-sugar [37], which is also under development against malignant glioma.

Since a critical point of G4 ligands design is their binding selectivity to G-quadruplex targets in comparison to the abundant duplex DNA, modulation of the basicity of the amine charged residues could be a promising strategy to investigate. Actually, the introduction as NDI side-chains of less basic morpholine groups instead of the strongly basic dimethyl amino groups could be really useful. In fact, the reduced basicity, reduces the positive charge on the ligand, limiting non-specific interactions, and enhancing its bioavailability [38].

In this work, we decided to explore several chemical modifications in carb-NDIs in order to improve efficacy, cytotoxicity and cellular uptake. Thus, we designed and prepared new carb-NDIs exploring novel glycosides (Carb-NDI-NMe2), modifying the dimethyl amine side-chains with morpholine moieties (Carb-NDI-morph), substituting *O*-glycosides with *S*-glycosides (Thiocarb-NDI-NMe2), and finally, NDIs merging both structural modifications (Thiocarb-NDI-morph) (Fig. 1). Then, we measured their antiproliferative and antiparasitic activity, their binding to G-quadruplexes, and their cellular and parasitic uptake.

2. Results and discussion

2.1. Design, synthesis and rationale

The design of these new carb-NDIs is based on the previously reported β-glc-*O*-C2-NDI-NMe2 **1** and α-man-*O*-C2-NDI-NMe2 **2** (Fig. 2) [21]. In this case, an ethylene glycol spacer was used to connect sugars to the NDI core through a triazole ring because this eight-atom chain length conjugating the NDI to the pyranose ring gave the best results in terms of cellular uptake. At the same time, carb-NDIs containing longer alkyl chains between the sugar and the central aromatic core resulted in less active antiparasitic agents against *Trypanosoma brucei* and *Leishmania major* than those found for compounds **1** and **2** [22]. Therefore, we have incorporated other mono- and disaccharides (galactose and maltose) through the ethylene glycol spacer used for **1** and **2**, yielding compounds **3** and **4**. We also synthesized the morpholine derived carb-NDIs version (compounds **5**–**8**). Then, the thioglycoside analogues (**9**–**16**) of the carb-NDIs **1**–**8** were prepared.

The library of carbohydrates-NDIs conjugates has been obtained following the synthetic protocol reported in our previous work [21]. The key step is the copper(I)-catalyzed azide alkyne cycloaddition, using an azidosugar and an NDI with an alkyne moiety. Alkyne-NDI precursors have been synthesized in three steps, starting with imidation of the dibromo-1,4,5,8-naphthalentetracarboxylic dianhydride, in presence of 3-(dimethylamino)-1-propylamine or 4-(2-aminoethyl)morpholine to generate the corresponding naphthalene diimides **20a-c** and **21a-c**, respectively (Scheme 1). The mixture obtained from this reaction was used for the following step without further purification. Nucleophilic aromatic substitution on the NDI core was carried out in the presence of an excess of propargylamine in acetonitrile and refluxed overnight (Scheme 1). Products **18** and **19** were isolated after purification using reverse phase column chromatography.

The 2-azidoethyl *O*-glycoside derivatives **30**–**33** were prepared as previously reported starting from the corresponding trichloroacetimidate derivative: β-glucose-C2 [21,39], α-mannose-C2 [21,40], β-galactose-C2 [39] and β-maltose-C2 derivatives [40] (Scheme 2). In the case of the 2-azidoethyl *S*-glycoside derivatives **42**–**45**, they were prepared from the peracetylated carbohydrates by treatment with thiourea and 1-bromo-2-chloroethane, subsequent reaction with sodium azide and final de-*O*-acetylation [41].

Finally, 2-azidoethyl *O*-glycoside derivatives **30**–**33** and 2-azidoethyl *S*-glycoside derivatives **42**–**45** were conjugated to the alkyne NDIs **18** and **19** through Huisgen cycloaddition reaction, following a standard protocol [21]. Briefly, the reaction was performed in the presence of catalytic $CuSO_4 \cdot 5H_2O$ and sodium ascorbate, in a 1:1 H_2O:^{t}BuOH solution. After 1 h, the solvents were evaporated and the crude was purified through reverse phase column chromatography yielding the NDIs **1**–**16** in good yields (Scheme 3).

2.2. Antiproliferative and antiparasitic activity

Cytotoxicity of carb NDIs **1**–**16** was evaluated in two different cell lines, MRC5 (healthy human lung fibroblast) and HT29 (colorectal adenocarcinoma), to investigate potential differences in bioactivity (Table 1). Some general trends can be envisioned from these results. In general, morpholino substituted carb-NDIs **5**–**8** and **13**–**16** showed lower toxicity compared to dimethyl amino carb-NDI derivatives **1**–**4** and **9**–**12** in both cell lines. The IC50 values obtained for the morpholino NDI derivatives were in the low-mid micromolar range, whereas for the dimethyl amino NDI derivatives were in the submicromolar or low micromolar range. This effect could be due to differences in the ability to enter cells, to

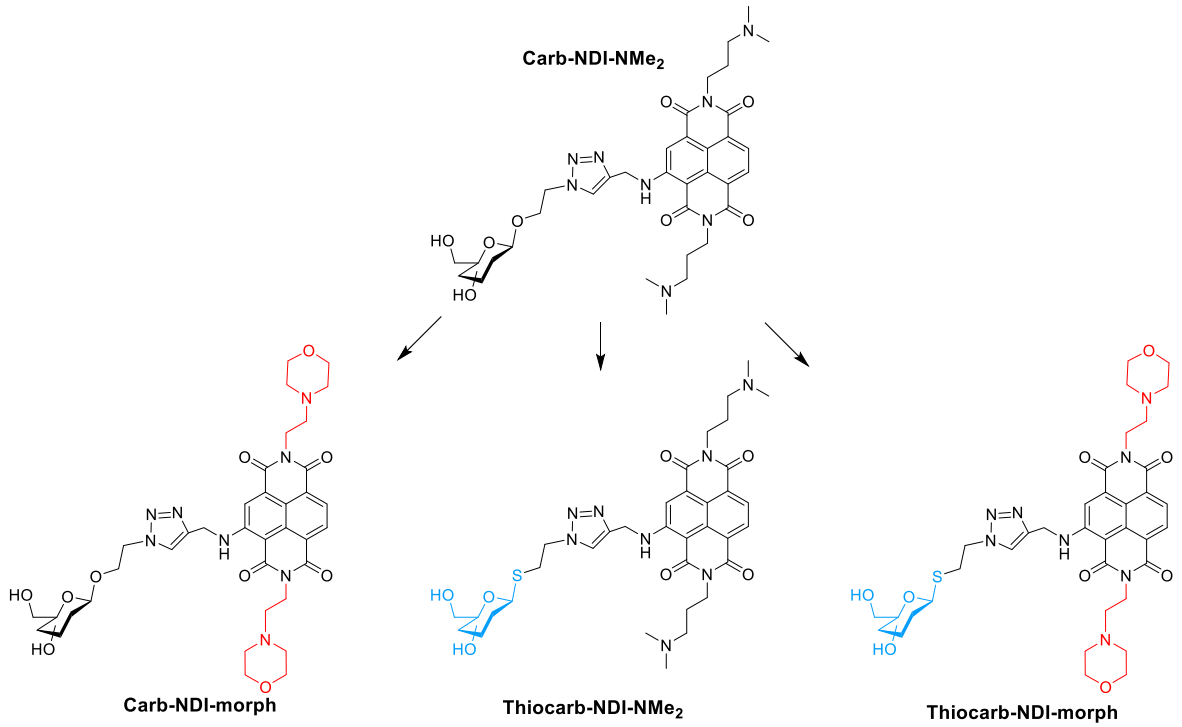

Fig. 1. Structures of carb-NDIs indicating the chemical modifications included in the compounds investigated in this study.

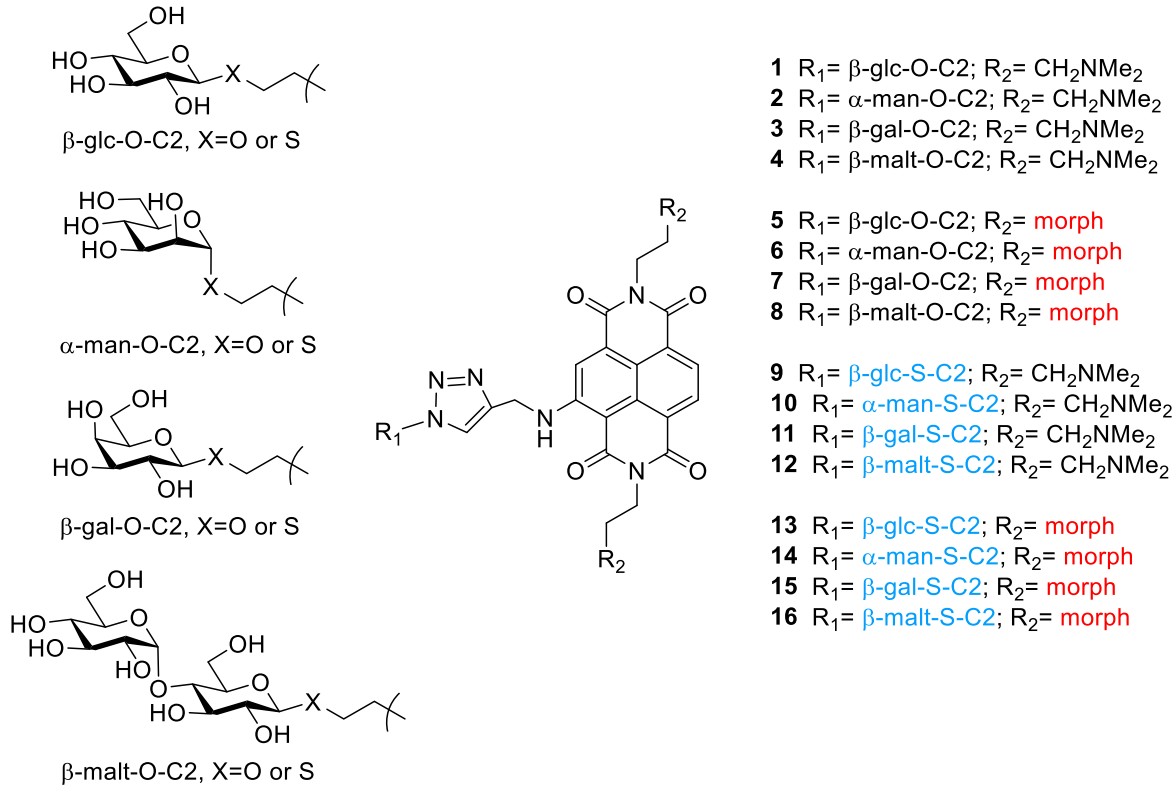

Fig. 2. Carbohydrate naphthalene diimide conjugates (Carb-NDIs **1**–**8**) and their thiosugar analogues (**9**–**16**) prepared in this work.

their binding efficacy to their potential targets (DNA G-quadruplexes) or to other factors.

The selectivity index (SI) was calculated by dividing IC50 values obtained for MRC-5 cells by those obtained for HT-29 cancer cells. We found that all carb-NDIs, except compound **15**, were more toxic against cancerous HT-29 cells than against non-cancerous MRC-5 cells. At the same time, *O*-glycoside NDIs tend to be more toxic than their *S*-glycoside NDI analogues against non-cancerous MRC-

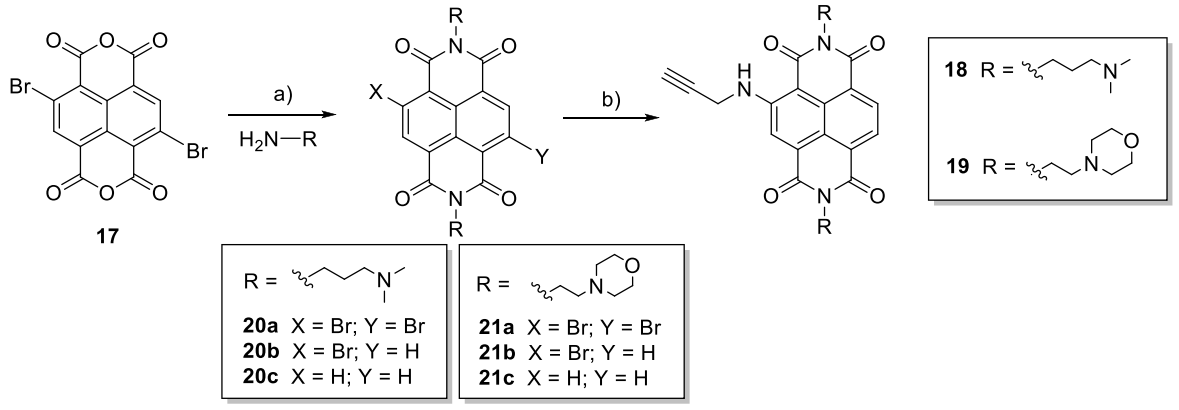

Scheme 1. Synthesis of alkyne-modified NDIs **18** and **19**. a) amine (3 eq.), acetic acid, reflux, 30 min; b) propargylamine (3 eq.), acetonitrile, reflux, 12 h.

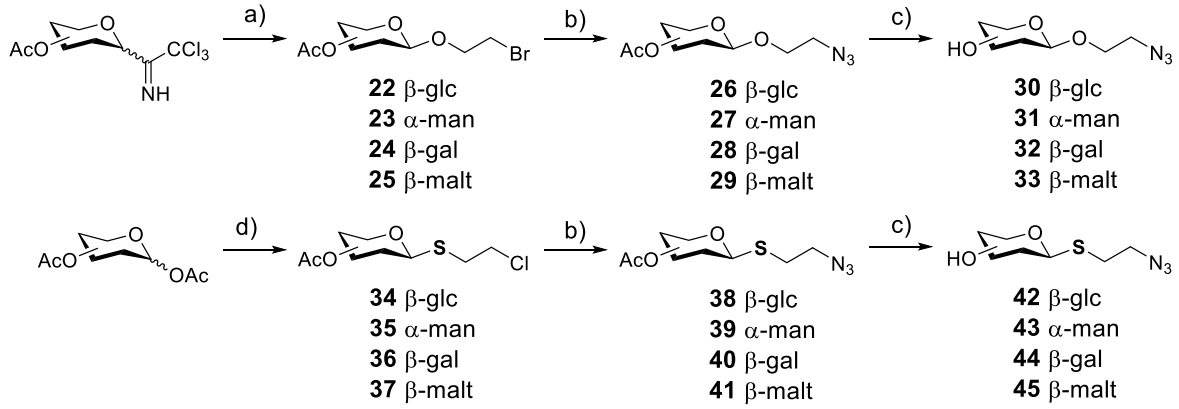

Scheme 2. Synthesis of 2-azidoethyl *O*-glycoside derivatives **30**–**33** and 2-azidoethyl *S*-glycoside derivatives **42**–**45**. a) 2-bromoethanol, $BF_3 \cdot Et_2O$, DCM; b) NaN3, DMF; c) NaOMe, MeOH; d) Thiourea, 1-bromo-2-chloroethane, $BF_3 \cdot Et_2O$, ACN.

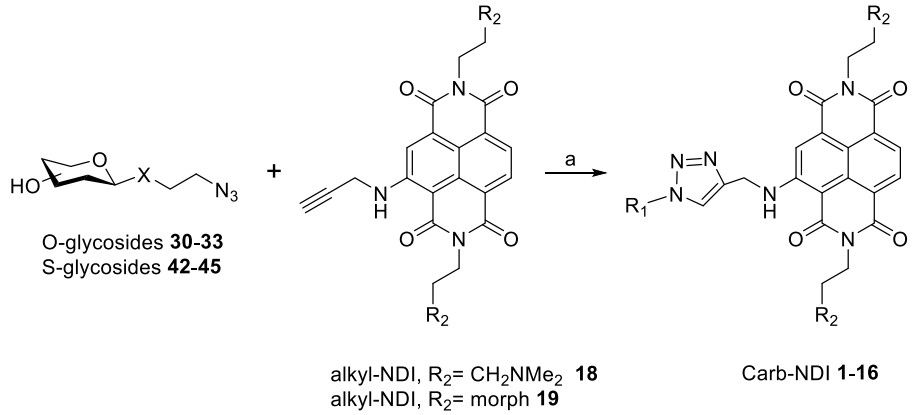

Scheme 3. Synthesis of carb-NDIs **1**–**16**. a) $CuSO_4 \cdot 5H_2O$, sodium ascorbate (1 eq.), *t*-BuOH/H_2O 1:1, r.t.,1 h.

5 cells. In fact, the most selective compound was the thiocarb-NDI derivative **12**, β-malt-S-C2-NDI-NMe_2, which resulted in an SI value of 9.8 fold. The rest of carb-NDIs showed SI values between 2 and 4 fold, except compound **14** with an SI value of 6.7. In the dimethyl amino carb-NDI series, the differences of cytotoxicity due to the carbohydrate moiety were small, with thiogalactosyl and thiomaltosyl derivatives being slightly more toxic than the other sugars against HT-29 cells. In the morpholino carb-NDI series, the differences of cytotoxicity due to the sugar unit were larger, with *O*-glucosyl, *O*-galactosyl and *S*-mannosyl derivatives around one order of magnitude more toxic than the rest of sugar derivatives against HT-29 and with smaller differences against MRC-5 cells.

The antiparasitic activity of carb NDIs **1**–**16** was measured against *Trypanosoma brucei* and *Leishmania major* promastigote parasites, and the SI value calculated by dividing the IC50 values obtained for MRC-5 cells by those obtained for *T. brucei* or *L. major*

Table 1
IC50 values measured for MRC-5 and HT-29 cells, *T. brucei*, *L. major* promastigotes , together with the resulting selectivity indexes, for compounds **1-16**. SI stands for selectivity index. Data in bold correspond to the best antiparasitic and antiproliferative activities.

	IC_{50} Parasites (μM)		IC_{50} Cells (μM)		SI		
	L. major	*T. brucei*	HT-29	MRC-5	*L. major*	*T. brucei*	HT-29
1 β-glc-O-C2-NDI-NMe_2	0.79 ± 0.15	0.08 ± 0.06	0.46 ± 0.09	0.92 ± 0.04	1.2	11.5	2.0
2 α-man-O-C2-NDI-NMe_2	0.30 ± 0.03	0.05 ± 0.02	0.43 ± 0.02	0.95 ± 0.43	3.2	19.0	2.2
3 β-gal-O-C2-NDI-NMe_2	13.9 ± 2.10	**0.05 ± 0.01**	0.50 ± 0.20	1.94 ± 0.65	1.4	**38.8**	3.9
4 β-malt-O-C2-NDI-NMe_2	0.80 ± 0.05	**0.06 ± 0.03**	0.48 ± 0.26	1.80 ± 0.52	2.3	**30.0**	3.8
5 β-glc-O-C2-NDI-morph	10.5 ± 1.37	0.31 ± 0.06	1.75 ± 0.50	7.86 ± 0.50	0.7	25.3	**4.5**
6 α-man-O-C2-NDI-morph	>50	2.10 ± 0.18	8.52 ± 4.25	30.5 ± 15.1	–	14.5	3.6
7 β-gal-O-C2-NDI-morph	27.5 ± 2.90	**0.15 ± 0.02**	3.60 ± 2.50	10.4 ± 3.24	1.3	**69.3**	2.9
8 β-malt-O-C2-NDI-morph	>50	3.32 ± 1.82	13.0 ± 5.18	>50	–	>15	>3.8
9 β-glc-S-C2-NDI-NMe_2	1.38 ± 0.55	**0.05 ± 0.02**	0.75 ± 0.11	2.75 ± 1.80	2.0	**55.0**	3.7
10 α-man-S-C2-NDI-NMe_2	1.52 ± 0.55	0.08 ± 0.06	0.88 ± 0.22	2.78 ± 2.15	1.8	34.7	3.2
11 β-gal-S-C2-NDI-NMe_2	0.74 ± 0.15	**0.04 ± 0.01**	**0.35 ± 0.12**	1.55 ± 0.23	2.1	**38.7**	**4.4**
12 β-malt-S-C2-NDI-NMe_2	0.51 ± 0.10	**0.06 ± 0.04**	**0.30 ± 0.10**	2.94 ± 0.38	5.7	**49.0**	**9.8**
13 β-glc-S-C2-NDI-morph	30.2 ± 2.11	1.18 ± 0.06	28.9 ± 0.82	35.7 ± 11.7	1.2	30.3	1.2
14 α-man-S-C2-NDI-morph	21.7 ± 1.28	0.73 ± 0.23	3.39 ± 0.62	22.6 ± 1.96	1.1	31.0	**6.7**
15 β-gal-S-C2-NDI-morph	30.0 ± 0.72	0.85 ± 0.29	26.5 ± 2.00	23.5 ± 6.30	0.8	27.6	0.9
16 β-malt-S-C2-NDI-morph	>50	3.04 ± 0.16	13.7 ± 1.08	>50	–	>16	>3.6

parasites. All the compounds showed higher efficacy against *T.brucei* than against *L. major* parasites, most probably due to the previously observed overall higher drug sensitivity of *T.brucei* than *L. major* [42,43]. At the same time, the general trend observed for the toxicity of carb-NDIs in mammalian cells is also observed against parasites. Thus, the morpholino substituted carb-NDIs **5**–**8** and **13**–**16** showed lower toxicity compared to dimethyl amino carb-NDI derivatives **1**–**4** and **9**–**12** in both parasites. In the case of the dimethyl amino carb-NDI's, the IC50 values found for *T.brucei* (0.04–0.08 μM) were all very similar, independently of the *O*- or *S*-glycoside present in the compound. In the case of *L. major*, the IC50 values were higher (0.3–1.5 μM) than those for *T.brucei*, with compound **3** being the least toxic one (13.9 μM). In the series of the morpholino carb-NDI's, the IC50 values found for *T.brucei* showed more variation (0.15–3.32 μM) depending on the carbohydrate unit, with *O*-glucosyl and *O*-galactosyl NDI morph derivatives being the most active ones. The IC50 data for *L. major* were in the mid-micromolar range indicating low toxicity against this parasite.

Concerning the selectivity index calculated for *L. major* over MRC-5 cells, the carb-NDI conjugates showed small SI values of up to 5.7. In contrast, the SI for *T. brucei* were higher (11.5–55), with β-gal-*O*-C2-NDI-morph **7** showing the highest selectivity of series (69-fold). This value is in the same range of that found for β-malt-*O*-TEG-NDI-NMe_2 reported recently by our group [22]. The TEG linker was $-(CH_2O)_3-$triazole$-(CH_2)_3-$NH- bound to the NDI scaffold modified with two dimethyl amino side chains.

2.3. Binding to G4 DNA

One of the potential targets of naphthalene diimides are DNA G-quadruplexes (G4). Thus, we evaluated the binding of several carb-NDIs to these relevant secondary DNA structures. Based on their biological activity, we selected compounds **3** and **4** (β-gal-*O*-C2-NDI-NMe_2 and β-malt-*O*-C2-NDI-NMe_2), and their thiosugars equivalents compounds **11** and **12** (β-gal-*S*-C2-NDI-NMe_2 and β-malt-*S*-C2-NDI-NMe_2), together with gal-NDI morpholino derivatives **7** and **15** (β-gal-*O*-C2-NDI-morph and β-gal-*S*-C2-NDI-morph), in order to compare the role of the amine group on binding.

First, we measured binding of the selected carb-NDI conjugates to the well known human telomeric sequence F21T [5′-d($G_3(T_2AG_3)_3$)-3’], also found in *T. brucei* and numerous mammalian species, using the FRET assay [44] (Fig. 3). We observed ΔTm values between 10 and 12 °C for the carb-NDI-NMe_2 (**3**, **4**, **11** and **12**), derivatives at 1 μM concentration, with few differences among them, whereas the carb-NDI-morph ligands (**7**, **15**) showed ΔTm's around 1–2 °C. These results seem to indicate that the lower basicity of the morpholine groups with respect to the dimethylamino groups may be the reason of the poor binding of compounds **7** and **15** to the DNA G-quadruplex. In fact, this is the case even at higher ligand concentration of **7** and **15** (2 and 5 μM concentration, respectively), rendering ΔTm values around 4–6 °C. These results seem to correlate with the lower toxicity found for carb-NDI-morph derivatives than for carb-NDI-NMe_2 derivatives, both in cells and parasites. At the same time, the small differences in ΔTm found for the carb-NDI's indicate that the carbohydrate does not play a relevant role on binding to the G-quadruplex, as we had observed previously for compounds **1** and **2** [21].

We also carried out FRET melting experiments under competing conditions of increasing concentrations of double stranded DNA (ds26, 3 and 10 eq, see Fig. S2) for four selected carb-NDI-NMe_2 ligands (**3**, **4**, **11** and **12**) to study their selectivity of G4 versus duplex DNA binding. We found a small but significant selectivity for G4s against DNA duplex. In the presence of 10 equivalents of ds26 competitor, a decrease of roughly 70–75% in the induced stabilization was observed for F21T.

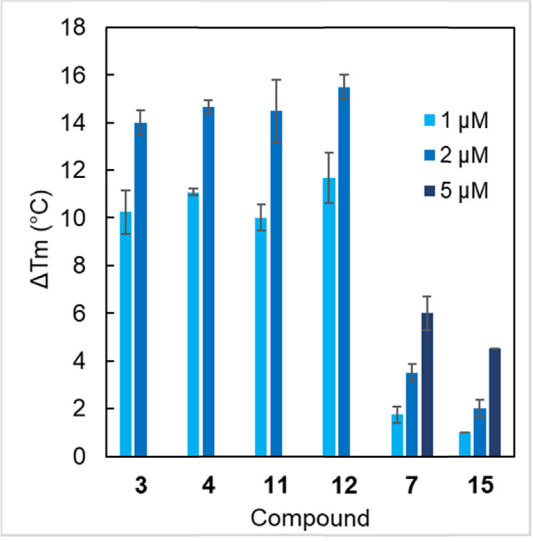

Fig. 3. FRET melting assays for compounds **1**–**16** with F21T G-quadruplex.

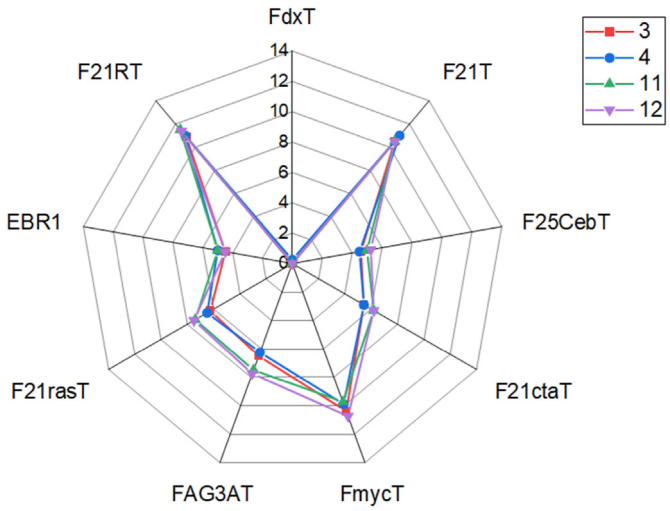

Fig. 4. FRET melting assays for compounds carb-NDIs **3** and **4**, and their corresponding thiocarb-NDIs **11** and **12** (at 1 μM conc.) with different G-quadruplexes.

In order to investigate potential G4 binding selectivity, we measured binding of carb-NDI-NMe_2 (**3**, **4**, **11** and **12**) to several G4 sequences. We selected as DNA G4s: EBR1, a sequence unique to *T. brucei* [10] with a hybrid topology, four sequences with parallel topology such as, F25CebT, the human *mini-satellite* G4 sequence, F21rasT, the Kras promoter, FAG3AT, a G4 synthetic construct and FmycT, and a sequence with antiparallel topology, F21ctaT. We also included an RNA G4, the human telomeric RNA F21RT and as control FdXT, a hairpin duplex with a hexaethyleneglycol loop (see Table S1 for sequences). ΔTm values at 1 and 2 μM ligand concentration are shown in Fig. 4 and Fig. S3, respectively. We observed F21T, its corresponding RNA G4, F21RT, and FmycT were found to be the sequences most stabilized by the carb-NDI NMe_2 ligands, whereas EBR1-FT and F25CebT showed the smallest stabilization of the selected G4's. It is important to mention that no stabilization was observed for the DNA duplex control FdxT. At the same time, only small differences on binding were found between the four sugar-NDI measured, independently of being O- or S-glycoside, pointing again to a negligible role of the carbohydrates on binding to the G-quadruplexes.

Next, we studied ligand binding to the G4 structures using native electrospray mass spectrometry, which will also provide the resulting stoichiometry [45]. The four selected carb-NDI-NMe_2 ligands were evaluated with several DNA sequences. These include the following ones: the human telomeric 22AG, [5′-$d(AG_3(T_2AG_3)_3)$-3'], the *T.brucei* G4 sequence EBR1, [5′-$d(G_3CAG_5TGATG_4AG_2AGC_2AG_3)$-3'], a parallel tetramolecular G4, [5′- $d(TG_4T)_4$-3'], a bimolecular antiparallel sequence [5′-$d(G_4T_4G_4)_2$-3'] and two duplex sequences, the Dickerson-Drew dodecamer [46], here noted d66 [5′-$d(CGCGA_2T2CGCG)_2$-3'], and self-complementary duplex with 100% CG-content [5′-$d((CGCG_3C_3GCG)_2)$-3']. The corresponding mass spectra are shown in Fig. 5 and Fig. S4.

We found all four carb-NDI NMe_2 compounds actually bind to quadruplexes and, in all cases, only 1:1 complexes were detected. It is important to note that the 1:1 complex of compound **12**, β-D-malt-*S*-C2-NDI-NMe_2, with the $(TG_4T)_4$ quadruplex is observed with 3 ammonium ions but also with 2 ammonium ions (see insertion on Fig. 3B). This could suggest a putative secondary interaction mode through intercalation with the displacement of one of the coordinated ammonium cations in the G4 structure. Among the quadruplex studied, the four carb-NDIs showed binding preference for parallel tetramolecular G4 $(TG_4T)_4$, except for compound **4**, β-D-malt-*O*-C2-NDI-NMe_2, with similar binding also to the human telomeric G4 (Fig. S4). Binding of the four sugar-NDIs to DNA duplexes d66 and d100 is also detected and, in some cases, even higher than that found to quadruplexes.

When the equilibrium binding constants were calculated using our previously reported methodology [47,48], all four ligands showed K_1 binding constants in the range of 5.9×10^4 M^{-1} to 4.1×10^5 M^{-1} with $(TG_4T)_4$ quadruplex, and in the range of $0.3–7.2 \times 10^4$ M^{-1} with the other three G4 studied (Table S2).

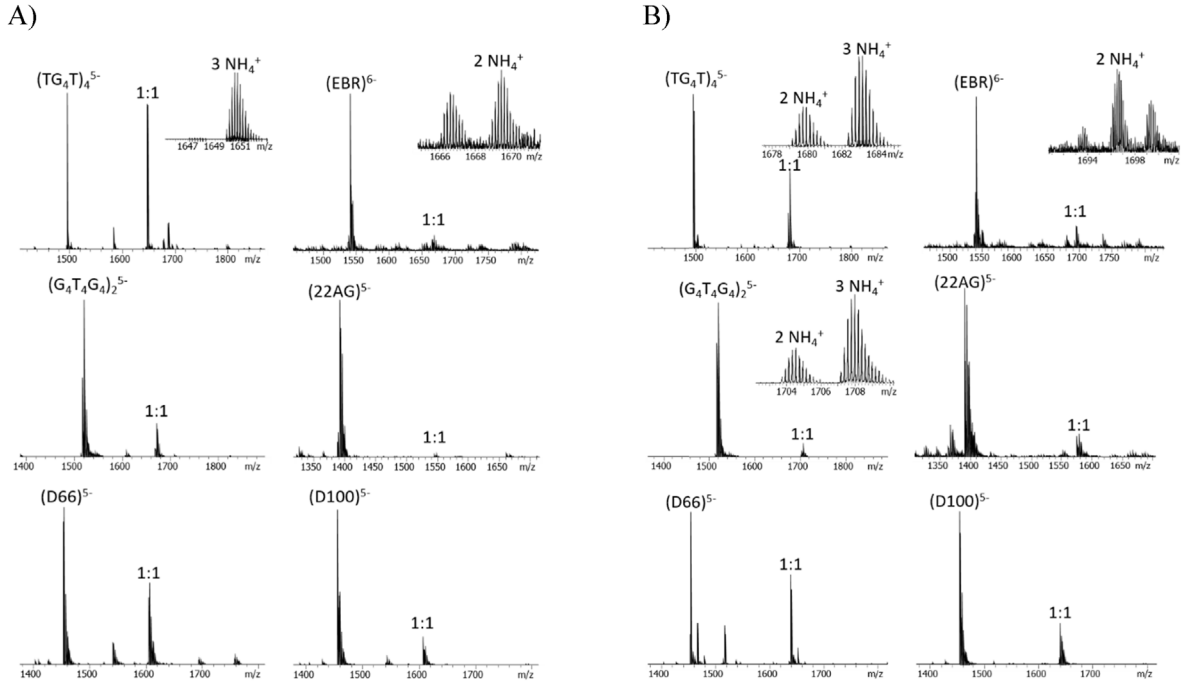

Fig. 5. Mass spectra for β-D-gal-*S*-C2-NDI-NMe_2, compound **11** (A) and for β-D-malt-*S*-C2-NDI-NMe_2 compound **12** (B) with different DNA G-quadruplexes and DNA duplexes.

Selectivity with respect to DNA duplex was smaller than expected, with K_1 binding constants ranging from 1.9×10^4 M^{-1} to 1.25×10^5 M^{-1}. This result may be due to a preference on binding to duplex regions rich on CG base pairs, since we did not observe such affinity to FdxT duplex, containing just one CG base pair when measured using the FRET assay. In fact, we carried out further FRET experiments for compounds **3**, **4**, **11** and **12** with control duplexes containing higher CG content (up to 30%) and ΔTm values obtained remained low (0–2 °C) (Fig. S5). It is important to note that a direct comparison between DNA binding studies measured through FRET and mass spectrometry can show biased results. As a matter of fact, studies on mechanism of action of this type of ligands indicate carb-NDIs actually bind G-quadruplexes in ribosomal DNA as demonstrated using fluoresecent intercalator displacement (FID) assay, NMR and a DNA polymerase stop assay on G4 sequences found in the rDNA [30]. At the same time, a fluorescence confocal microscopy displacement experiment run with thioflavin T (ThT), a fluorescent light-up probe of ribosomal G4s in the nucleolus, run on SW480 cells, showed that carb-NDI sharply decreased the ThT-stained foci, indicating that carb-NDI displaced ThT from the nucleolar G4s. Thus, carb-NDIs exhibited a G4-binding pattern inside cells mainly targeting G4s in the nucleolar rDNA.

2.4. Cellular and parasitic uptake of carb-NDI conjugates

We evaluated cell entrance of several *O*- and *S*-glycoside-NDI-NMe_2, and compared it to that of the corresponding carb-NDI-morph analogues (Table 2). We took advantage of the red fluorescent emission of NDI derivatives to monitor their cell entry [21]. Fluorescence spectroscopy measurements were made to study their entrance within a cancer cell line (human colon adenocarcinoma HT-29, a noncancerous cell line (human lung fibroblast MRC-5) and *T. brucei* epimastigotes. They were carried out exciting the red dye at λ = 485 nm and recording its emission at λ = 535 nm after incubation with the compounds (10 μm) for 2 h.

Table 2
Cell uptake of selected carb-NDIs and control NDIs. Percentage of compound entering the cells of total incubated. The symbol (–) means data not measured.

	HT-29	MRC-5	*T. brucei*
2 α-man-O-C2-NDI-NMe_2	–	–	8.1 ± 1.1
4 β-malt-O-C2-NDI-NMe_2	20.9 ± 9.0	25.5 ± 13.5	7.0 ± 0.5
6 α-man-O-C2-NDI-morph	–	–	4.2 ± 1.0
7 β-gal-O-C2-NDI-morph	–	–	5.4 ± 0.9
8 β-malt-O-C2-NDI-morph	3.2 ± 2.4	0.8 ± 0.2	6.1 ± 2.0
10 α-man-S-C2-NDI-NMe_2	–	–	6.1 ± 1.4
12 β-malt-S-C2-NDI-NMe_2	23.1 ± 13.9	20.7 ± 18.5	4.3 ± 0.7
14 α-man-S-C2-NDI-morph	–	–	3.2 ± 0.1
15 β-gal-S-C2-NDI-morph	–	–	6.8 ± 0.3
16 β-malt-S-C2-NDI-morph	3.5 ± 0.4	3.3 ± 3.4	6.7 ± 0.6

In the case of *T. brucei*, a small percentage of the carb-NDI entered the parasites (3.2–8.1%), with small differences between the sugar or the tertiary amine modifying the structure, that, in any case, was higher than two fold. In contrast, compounds **4** and **12** (β-malt-*O*-C2-NDI-NMe_2 and β-malt-*S*-C2-NDI-NMe_2), enter both HT-29 and MRC-5 cells in much higher percentage (20.7–25.5%) than their morpholine-NDI counterparts, compounds **8** and **16** (β-malt-*O*-C2-NDI-morph and β-malt-*S*-C2-NDI-morph), with only a 0.8–3.5% entrance. These results correlate quite well with the cytotoxicity found in mammalian cells where NMe_2-NDIs were much more toxic than the morph-NDIs, independently of the sugar substituent.

Next, we used confocal microscopy to study the localization of compounds **4** and **12** (β-malt-*O*-C2-NDI-NMe_2 and β-malt-*S*-C2-NDI-NMe_2) in HT-29 cells and in T. brucei parasites, exploiting again its intrinsic fluorescence properties. In the case of HT-29 cancer cells, we observed both carb-NDIs mainly co-localized with the DNA probe DAPI highlighting its preferential distribution in the nucleus (Fig. 6), with no differences among them. In the case of *T. brucei*, compounds **4** and **12** could be localized in the nucleus but also in other areas of the cytoplasm (Fig. S6). This is in contrast with our previous results with other carb-NDIs [21] and could be due to a short incubation time.

3. Conclusions

We have explored the influence of different amino side chains such as dimethylamino and morpholino, together with a variety of *O*- and *S*-glycosides attached to NDIs on their bioactivity and their G-quadruplex binding ability. Carb-NDI-NMe_2 derivatives turned out to be more potent antiproliferative and antiparasitic agents than their carb-NDI-morph analogues. The reasons behind these differences seem to be poorer G4 binding of carb-NDI-morph ligands, besides their low cellular uptake in comparison with that of the carb-NDI-NMe_2 derivatives.

The main observed difference with respect to their bioactivity between *O*-carb-NDI-NMe_2 and *S*-carb-NDI-NMe_2 is the fact that thiocarb-NDIs were overall less toxic against MRC-5 cells. This leads to a higher selectivity index for these *S*-carb-NDI-NMe_2 derivatives. For example, compound **12** (β-malt-*S*-C2-NDI-NMe_2) displays potent growth inhibition activity against colon cancer cells, at sub-μM concentrations, and shows great selectivity against control human fibroblasts (9.8-fold) which is the best reported one for carb-NDI derivatives.

In the case of *T. brucei* parasites, several carb-NDI-NMe_2 displayed nanomolar activity with a good selectivity index, in the range of 30- to 55-fold. However, the best SI (69-fold) was observed for compound **7**, β-gal-*O*-C2-NDI-morph. Finally, we confirmed binding of carb-NDI's to quadruplexes using different biophysical measurements, although the G4 selectivity *vs* duplex DNA was smaller than expected. Finally, carb-NDI localization was studied by confocal microscopy, and whereas compounds **4** and **12** (β-malt-*O*-C2-NDI-NMe_2 and β-malt-*S*-C2-NDI-NMe_2 were located in the HT-29 cell nucleus, they were also found in both the cytoplasm and nucleus of *T. brucei* epimastigotes, probably due to short incubation times.

4. Experimental section

4.1. General materials and methods

Reagents, solvents and chemicals were purchased from Alfa Aesar or Sigma-Aldrich and were used as supplied without further

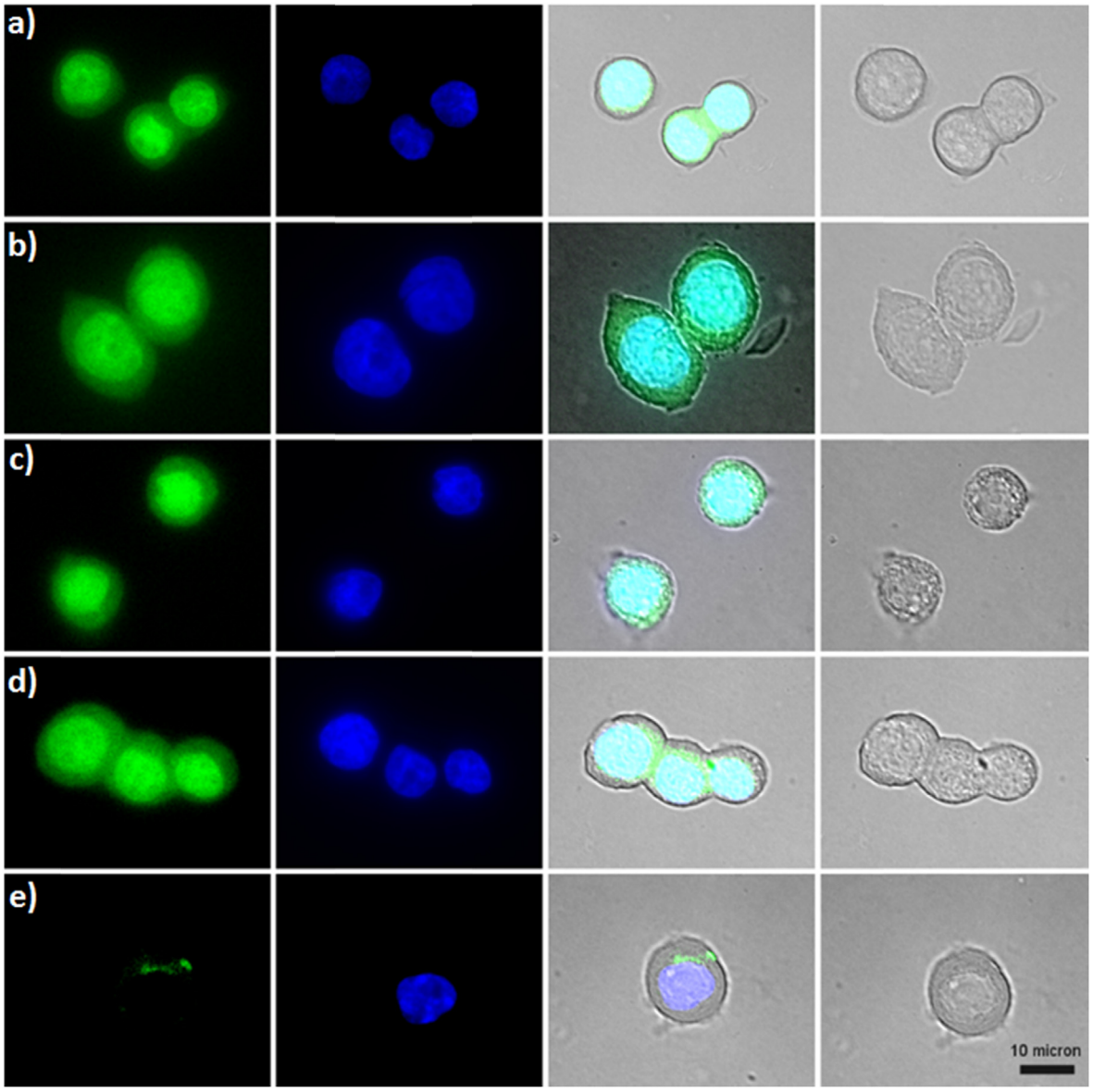

Fig. 6. Fluorescence microscopy of compounds **4** and **12**, β-malt-*O*-C2-NDI-NMe_2 and β-malt-*S*-C2-NDI-NMe_2, respectively, in HT-29 cancer cells. Left to right columns: fluorescence of the compounds at 25uM concentration, DAPI staining, merge image and light microscopy image, respectively. A) compound **4**, 30 min, B) compound **4**, 2h, C) compound **12**, 30 min, D) compound **12**, 2h, E) Negative control.

purification. Oligonucleotides were purchased from Eurogentec and were used without further purification. Oligonucleotide stock solutions (about 5×10^{-4} M) were prepared in MilliQ water and stored at − 20 °C. The exact stock concentrations were determined from the absorbance at 260 nm. The ODNs were annealed by incubation at 95 °C for 5 min and letting them cool down at r.t to promote the folding. Heating was carried out using a thermoblock (Accublock by Labnet). The folded samples were then stored, at 4 °C, if necessary. The compounds were solubilized in water at 1×10^{-2} M concentration and stored at −20 °C. TLC analysis was carried out on silica gel (Merck 60F-254) with visualization at 254 and 366 nm or with the appropriate stainers. The solvents used for all the HPLC analyses and purifications were 0.1% trifluoroacetic acid in water and acetonitrile. HPLC analysis was performed using an Agilent system SERIES 1260. The column was XSelectHSS C18 (2.5 μm) (4.6 × 50 mm) (Waters). The following analytical method (method 1) was used, flow: 1.4 mL/min; gradient: 95% aqueous solution, gradually to 40% aqueous solution over 8 min and then isocratic flow for 4 min; (method 2) was used, flow: 1.4 mL/min; gradient: 95% aqueous solution, gradually to 40% aqueous solution over 12 min and then isocratic flow for 4 min.

Preparative reverse phase purification of NDI precursors and carb-NDI conjugates was carried out using an Agilent Technologies 1260 Infinity preparative HPLC, provided with a diode array UV−vis detector. The column was a SunFire C18 OBD (5 μm, 150 × 30 mm). The following method was used for the purification of NDIs (method 3): flow: 30 mL/min; gradient: 95% of aqueous solvent, then gradually to 70% aqueous over 5 min, then to 40% aqueous over 13 min and then isocratic flow for 2 min (λ detection: 620, 530 and 256 nm). The following method was used for the purification of carb-NDI conjugates (method 4): flow: 30 mL/min; gradient: 85% of aqueous solvent, then gradually to 70% aqueous over 12 min, then to 50% aqueous over 2 min and finally isocratic flow for 3 min (λ detection: 530, 450 and 256 nm). ^{1}H NMR and ^{13}C NMR spectra were recorded on a Bruker NMR equipment.

4.2. Synthesis

4.2.1. Synthesis of NDI intermediates compounds **20a-20c** and alkyne-NDI derivatives **18**

These compounds were synthesized from compound **17** according to the published synthetic protocol [21].

4.2.2. Synthesis of NDI intermediates compounds **21a-21c**

In a one-necked flask, 500 mg (1.18 mmol, 1 eq.) of dibromo-naphthalene diimide **17**, previously synthesized according to a published procedure [21], were suspended into 100 ml of acetic acid. Then, 0.460 ml (3.54 mmol, 3 eq.) of 4-(2-aminoethyl)morpholine were added to the mixture. The solution was refluxed for 30 min, under nitrogen atmosphere, and then neutralized through addition of sodium hydrogen carbonate. The crude was extracted three times with dichloromethane (3 × 200 ml) and used for the next step without further purification.

4.2.3. Synthesis of alkyne-NDI derivative **19**

In a round bottomed flask, 300 mg (0.46 mmol, 1 eq.) of dibromo-naphthalene diimide **21a** were dissolved into 150 ml of acetonitrile, and 0.08 ml propargylamine (1.39 mmol, 3 eq.) were added. The reaction mixture was refluxed for 12 h, and then the solvent was removed under reduced pressure. The crude was purified using reverse phase column chromatography and 100 mg (Yield = 40%, red solid) of pure product **19** were isolated. ^{1}H NMR (300 MHz, D2O) δ ppm 8.16 (d, J = 7.8 Hz, 1H), 7.98 (d, J = 7.9 Hz, 1H), 7.9 (s, 1H), 4.48–4.42 (m, 4H), 4.3 (s, 2H), 4.02 (m, 4H), 3.69–3.65 (m, 8H), 3.5–3.45 (m, 4H), 3.22–3,19 (m, 4H), 2.82 (s, 1H). ^{13}C NMR (75 MHz, D2O): δ ppm 168.59; 167.27; 167.05; 166.67; 154.70; 134.67; 131.69; 129.94; 128.46; 128.34; 125.74; 123.67; 121.95; 102.97; 82.22; 77.35; 66.99; 58.10; 57.83; 55.62; 38.18; 37.67; 35.86. HRMS (ESI): m/z calculated for $C_{29}H_{31}N_5O_6$+H^+: 546.2347 $[M+H]^+$; found: 546.3216.

4.2.4. Protocol for step a of Scheme 2

To a solution of peracetylated 1-trichloroacetimidate sugar (1 eq.) in anhydrous DCM, under argon atmosphere, 2-bromo ethanol (1.1 eq.) was added dropwise. Boron trifluoride diethyl etherate was then added (1 eq.) and the reaction was stirred at room temperature for 30 min. After TLC verification of total consumption of the initial product, 10% aqueous solution of Na_2CO_3 was added. The organic phase was washed three times (3 x 100 mL) with the basic solution, concentrated and purified through flash column chromatography, using, as eluent, a mixture of Hexane: Ethyl Acetate 4:1 to 2:1.

Compounds **22** and **23** were synthesized according to the published synthetic protocol [21].

Compound **24**. 2-Bromoethyl 2,3,4,6-tetra-*O*-acetyl-β-D-galactopyranose. Yield = 37%, Rf = 0.25 (Hexane: Ethyl Acetate – 2:1). The compound characterization coincided with the description found in literature [39].

Compound **25**. 2-Bromoethyl 2,3,4,2′,3′,4′,6′-hepta-*O*-acetyl-β-D-maltopyranose, Yield = 13%, Rf = 0.2 (Hexane: Ethyl Acetate – 2:1), which was fully characterized according to the literature [40].

4.2.5. Protocol for step b of Scheme 2

Solution of 2-bromoethyl *O*-glycoside or 2-chloroethyl *S*-glycoside (1 eq.) and sodium azide (10 eq.) in DMF (25 mL) was stirred for 24 h–96 h at room temperature. The reaction mixture was then diluted with DCM and extracted with water (6 x 100 mL) to yield the corresponding 2-azidoethyl glycosides.

Compounds **26** and **27** were synthesized according to the published synthetic protocol [21].

Compound **28**. 2-azidoethyl 2,3,4,6-tetra-*O*-acetyl-β-D-galactopyranose. Yield = 94%, which was fully characterized according to the literature [39].

Compound **29**. 2-azidoethyl 2,3,4, 2′,3′,4′,6′-hepta-*O*-acetyl-β-D-maltopyranose. Yield = 93%, which was fully characterized according to the literature [40].

Compound **38**. 2-azidoethyl 2,3,4,6-tetra-*O*-acetyl-β-D-1-thioglucopyranose. Yield = 50%. ^{1}H NMR (500 MHz, $CDCl_3$) δ 5.23 (t, J = 9.4 Hz, 1H), 5.06 (dt, J = 19.3, 9.7 Hz, 2H), 4.56 (d, J = 10.0 Hz, 1H), 4.19 (ddd, J = 14.7, 12.4, 3.7 Hz, 2H), 3.73 (ddd, J = 10.1, 5.0, 2.3 Hz, 1H), 3.60–3.43 (m, 2H), 2.95 (dt, J = 13.9, 6.9 Hz, 1H), 2.77 (dt, J = 13.9, 6.9 Hz, 1H), 2.09 (s, 3H), 2.06 (s, 3H), 2.03 (s, 3H), 2.01 (s, 3H). ^{13}C NMR (126 MHz, $CDCl_3$) δ 170.55, 170.08, 169.40, 169.36, 83.48, 76.05, 73.66, 69.62, 68.19, 62.02, 51.56, 29.43, 20.69, 20.66, 20.57, 20.55. TOF MS ES $^{+}$ Calculated mass $C_{16}H_{23}N_3O_9S$ [M + Na] = 456.1053, Found mass [M + Na] = 456.1048.

Compound **39**. 2-azidoethyl 2,3,4,6-tetra-*O*-acetyl-α-D-1-thiomannopyranose. Yield = 60%, which was fully characterized according to the literature [49].

Compound **40**. 2-azidoethyl 2,3,4,6-tetra-*O*-acetyl-β-D-1-thiogalactopyranose. Yield = 99%. ^{1}H NMR (300 MHz, $CDCl_3$) δ 5.37 (d, J = 2.6 Hz, 1H), 5.22–4.93 (m, 2H), 4.54 (d, J = 9.8 Hz, 1H), 4.04 (t, J = 8.3 Hz, 2H), 3.95 (t, J = 6.3 Hz, 1H), 3.66 (dt, J = 9.6, 5.7 Hz, 1H), 3.46 (ddd, J = 12.3, 7.8, 4.5 Hz, 1H), 3.14–2.95 (m, 1H), 2.72 (dd, J = 13.9, 7.0 Hz, 1H), 2.09 (s, 3H), 2.00 (s, 3H), 1.98 (s, 3H), 1.91 (s, 3H). ^{13}C NMR (75 MHz, $CDCl_3$) δ 170.39, 170.22, 169.99, 169.67, 83.97, 74.70, 71.81, 67.50, 61.77, 51.64, 43.51, 29.60, 20.84, 20.71, 20.63. TOF MS ES $^{+}$ Calculated mass for $C_{16}H_{23}N_3O_9S$ [M + H] = 434.1233, Found mass [M + H] = 434.1239.

Compound **41**. 2-azidoethyl 2,3,4, 2′,3′,4′,6′-hepta-*O*-acetyl-β-D-1-thiomaltopyranose. Yield = 43%. ^{1}H NMR (300 MHz, $CDCl_3$) δ 5.44–5.21 (m, 3H), 5.03 (t, J = 9.8 Hz, 1H), 4.90–4.79 (m, 2H), 4.64–4.45 (m, 2H), 4.28–4.13 (m, 2H), 4.13–3.90 (m, 3H), 3.75–3.57 (m, 2H), 3.48 (dd, J = 10.6, 6.4 Hz, 1H), 3.10–2.65 (m, 2H), 2.12 (s, 3H), 2.08 (s, 3H), 2.04–1.97 (m, 15H). ^{13}C NMR (75 MHz, $CDCl_3$) δ 170.72, 170.67, 170.57, 170.24, 170.08, 169.77, 169.59, 95.85, 83.37, 72.78, 70.80, 70.19, 69.48, 68.80, 68.21, 62.99, 61.71, 51.75, 43.54, 32.61, 29.81, 21.09, 20.98, 20.96, 20.88, 20.83, 20.78, 20.78. TOF MS ES $^{+}$ Calculated mass for $C_{28}H_{39}N_3O_{17}S$ [M + Na] = 744.1898, Found mass [M + Na] = 744.1863.

4.2.6. Protocol for step c of Scheme 2

In a round-bottom flask, the protected 2-azidoethyl glycoside (1 eq.) was dissolved in MeOH. A solution of sodium methoxide (2 mL/1 mmol of protected sugar, 25% v/v in MeOH) was added dropwise and stirred until TLC verification showed complete transformation of the starting material. Solvents were evaporated and the resulting oil was resuspended in MeOH, then Amberlite ® 120H resin was introduced into the flask. The suspension was stirred until pH = 7, then resin was filtered off. Evaporation of the solvents afforded the pure product as a yellow oil or foam.

Compounds **30** and **31** (2-azidoethyl β-D-glucopyranose and 2-azidoethyl α-D-mannopyranose) were synthesized according to the published synthetic protocol [21].

Compound **32**. 2-azidoethyl β-D-galactopyranose. Yield = 92%. ^{1}H NMR (400 MHz, CD_3OD) δ 4.31 (d, J = 6.9 Hz, 1H), 4.03 (dd, J = 10.8, 5.2 Hz, 1H), 3.88 (s, 1H), 3.79–3.73 (m, 3H), 3.59–3.55 (m, 1H), 3.54 (d, J = 2.9 Hz, 2H), 3.50 (t, J = 5.2 Hz, 2H). ^{13}C NMR (101 MHz, CD_3OD) δ 103.60, 75.24, 73.51, 71.11, 68.88, 67.92, 61.11, 50.78. TOF MS ES $^{+}$ Calculated mass for $C_8H_{15}N_3O_6$ [M + Na] = 272.0859, Found mass [M + Na] = 272.0835.

Compound **33**. 2-azidoethyl β-D-maltopyranose. Yield = 89%. ^{1}H NMR (400 MHz, CD_3OD) δ 4.98 (s, 2H), 4.41 (dd, J = 11.5, 7.3 Hz, 2H), 4.02 (dd, J = 10.7, 5.2 Hz, 1H), 3.91 (d, J = 9.6 Hz, 2H), 3.79 (dd, J =

11.5, 6.5 Hz, 2H), 3.65 (d, J = 8.1 Hz, 2H), 3.62–3.55 (m, 4H), 3.50 (t, J = 5.1 Hz, 2H), 3.33 (d, J = 1.4 Hz, 1H). ^{13}C NMR (101 MHz, CD_3OD) δ 178.61, 103.82, 102.77, 79.33, 75.69, 75.16, 73.32, 71.03, 68.96, 68.02, 61.13, 50.68, 48.55, 22.54. TOF MS ES $^+$ Calculated mass for $C_{14}H_{25}N_3O_{11}$ [M + Na] = 434.1387, Found mass [M + Na] = 434.1363.

Compound **42**. 2-azidoethyl β-D-1-thioglucopyranose. Yield = 97%. ^{1}H NMR (300 MHz, CD_3OD) δ 4.46 (d, J = 9.7 Hz, 1H), 3.89 (d, J = 11.9 Hz, 1H), 3.68 (dd, J = 11.6, 3.6 Hz, 1H), 3.57 (dt, J = 9.1, 5.9 Hz, 2H), 3.38 (d, J = 8.5 Hz, 1H), 3.34 (s, 2H), 3.23 (t, J = 9.0 Hz, 1H), 2.99 (dt, J = 13.9, 7.0 Hz, 1H), 2.91–2.78 (m, 1H). ^{13}C NMR (75 MHz, CD_3OD) δ = 85.82, 80.63, 78.14, 73.01, 70.07, 61.50, 51.52, 29.07. TOF MS ES $^+$ Calculated mass for $C_8H_{15}N_3O_5S$ [M + Na] = 288.0630, Found mass [M + Na] = 288.0605.

Compound **43**. 2-azidoethyl α-D-1-thiomannopyranose. Yield = 95%. ^{1}H NMR (300 MHz, CD_3OD) δ 5.34 (s, 1H), 3.98–3.83 (m, 2H), 3.83–3.70 (m, 2H), 3.70–3.65 (m, 2H), 3.56 (ddd, J = 12.9, 8.7, 4.8 Hz, 1H), 3.45–3.36 (m, 1H), 2.99–2.77 (m, 2H). ^{13}C NMR (75 MHz, CD_3OD) δ = 85.46, 73.74, 72.16, 71.69, 67.41, 61.34, 50.85, 30.04. TOF MS ES $^+$ Calculated mass for $C_8H_{15}N_3O_5S$ [M + Na] = 288.0630, Found mass [M + Na] = 288.0630.

Compound **44**. 2-azidoethyl β-D-1-thiogalactopyranose. Yield = 95%. ^{1}H NMR (400 MHz, CD_3OD) δ 4.41 (d, J = 9.1 Hz, 1H), 3.93 (d, J = 2.2 Hz, 1H), 3.74 (dd, J = 10.3, 6.1 Hz, 3H), 3.61–3.52 (m, 4H), 2.98 (dd, J = 13.8, 6.8 Hz, 1H), 2.91–2.77 (m, 1H). ^{13}C NMR (101 MHz, CD_3OD) δ 86.30, 79.18, 74.74, 70.02, 69.10, 61.29, 51.58, 29.12. TOF MS ES $^+$ Calculated mass for $C_8H_{15}N_3O_5S$ [M + Na] = 288.0630, Found mass [M + Na] = 288.0629.

Compound **45**. 2-azidoethyl β-D-1-thiomaltopyranose. Yield = 43%. ^{1}H NMR (400 MHz, MeOD) δ = 5.21 (d, J = 3.4 Hz, 1H), 4.48 (d, J = 9.7 Hz, 1H), 3.94–3.78 (m, 4H), 3.75–3.54 (m, 6H), 3.50–3.42 (m, 2H), 3.34–3.25 (m, 2H), 3.03–2.92 (m, 1H), 2.86 (dt, J = 13.8, 6.8 Hz, 1H). 13C NMR (101 MHz, MeOD) δ = 101.39, 85.76, 79.21, 77.91, 73.69, 73.35, 72.73, 70.08, 61.34, 60.99, 51.51, 43.48, 32.30, 29.12. TOF MS ES $^+$ Calculated mass for $C_{14}H_{25}N_3O_{10}S$ [M + Na] = 450.1158, Found mass [M + Na] = 450.1140.

4.2.7. Protocol for step d of Scheme 2

It follows a modification of the procedure described in Morales-Sanfrutos et al. [41]. Briefly, to a solution of the peracetylated sugar (1 eq.) and thiourea (1.1 eq.) in dry acetonitrile (10 mL) was added $BF_3{\cdot}Et_2O$ (2 eq.). The reaction mixture was then refluxed for 3 h. After cooling 1-bromo-2-chloroethane (2.5 eq.) and NEt_3 (4 eq.) were added and the reaction mixture was magnetically stirred at r.t. for 12 h. Then, the solvent was evaporated under vacuum to give a crude that was dissolved in DCM (100 mL) and washed with water (3 x 100 mL). The organic phase was evaporated and purified by flash column chromatography using as eluents Hexane: Ethyl Acetate − 4:1 to 2:1.

Compound **34**. 2-chloroethyl 2,3,4,6-tetra-*O*-acetyl-β-D-1-thioglucopyranose, which was fully characterized according to the literature [41].

Compound **35**. 2-chloroethyl 2,3,4,6-tetra-*O*-acetyl-α-D-1-thiomannopyranose. Yield = 49%, R_f = 0.5 (Hexane: Ethyl Acetate − 1:1). ^{1}H NMR (300 MHz, $CDCl_3$) δ = 5.24 (s, 1H), 5.22–5.10 (m, 2H), 4.38–4.26 (m, 1H), 4.22 (dd, J = 11.9, 6.2 Hz, 1H), 4.05 (dd, J = 12.0, 1.5 Hz, 1H), 3.80–3.37 (m, 3H), 3.04–2.83 (m, 2H), 2.09 (s, 3H), 2.03 (s, 3H), 1.99 (s, 3H), 1.92 (s, 3H). ^{13}C NMR (75 MHz, $CDCl_3$) δ = 170.68, 170.05, 169.94, 169.88, 83.28, 70.87, 69.46, 69.41, 66.40, 62.67, 42.85, 34.08, 21.01, 20.85, 20.76. TOF MS ES $^+$ Calculated mass for $C_{16}H_{23}ClO_9S$ [M + Na] = 449.0649, Found mass [M + Na] = 449.0666.

Compound **36**. 2-chloroethyl 2,3,4,6-tetra-*O*-acetyl-β-D-1-thiogalactopyranose. Yield = 18%, R_f = 0.25 (Hexane: Ethyl Acetate − 2:1). ^{1}H NMR (300 MHz, $CDCl_3$) δ = 5.37 (d, J = 2.4 Hz, 1H), 5.16 (t, J = 9.9 Hz, 1H), 5.00 (dd, J = 10.0, 3.0 Hz, 1H), 4.51 (d, J = 9.8 Hz, 1H), 4.13–3.98 (m, 2H), 3.92 (t, J = 6.3 Hz, 1H), 3.74–3.55 (m, 2H), 3.13–2.77 (m, 2H), 2.10 (s, 3H), 2.00 (s, 6H), 1.92 (s, 3H). ^{13}C NMR (75 MHz, $CDCl_3$) δ = 170.52, 170.29, 170.10, 169.70, 84.53, 74.82, 71.87, 67.50, 67.23, 61.87, 43.53, 32.97, 20.92, 20.81, 20.72. TOF MS ES $^+$ Calculated mass for $C_{16}H_{23}ClO_9S$ [M + H] = 427.0830, Found mass [M + H] = 427.0812.

Compound **37**. 2-chloroethyl 2,3,4,6-tetra-*O*-acetyl-β-D-1-thiomaltopyranose. Yield = 27%, R_f = 0.55 (Hexane: Ethyl Acetate − 1:1). ^{1}H NMR (300 MHz, $CDCl_3$) δ = 5.29 (ddd, J = 18.6, 9.6, 6.5 Hz, 3H), 4.99 (t, J = 9.8 Hz, 1H), 4.86–4.76 (m, 2H), 4.63–4.42 (m, 1H), 4.17 (ddd, J = 16.9, 12.3, 4.4 Hz, 2H), 4.07–3.87 (m, 3H), 3.76–3.50 (m, 3H), 3.38 (dt, J = 31.3, 7.7 Hz, 1H), 3.10–2.75 (m, 2H), 2.08 (d, J = 7.9 Hz, 3H), 2.04 (s, 3H), 1.97 (dd, J = 8.8, 3.8 Hz, 15H). ^{13}C NMR (75 MHz, $CDCl_3$) δ = 170.74, 170.64, 170.25, 170.12, 169.80, 169.63, 95.85, 83.49, 72.90, 70.74, 70.20, 69.46, 68.77, 68.21, 62.97, 61.76, 43.57, 42.35, 32.71, 32.27, 25.61, 21.07, 20.96, 20.87, 20.80, 20.76. TOF MS ES $^+$ Calculated mass for $C_{28}H_{39}ClO_{17}S$ [M + Na] = 737.1494, Found mass [M + Na] = 737.1469.

4.2.8. Protocol for step a of Scheme 3

a) Carb-NDIs **1**–**4** and **9**–**12.** A solution of (+)-sodium-L-ascorbate (12 mg, 0.06 mmol), copper(II) sulfate pentahydrate (1.5 mg, 0.006 mmol) and alkynyl NDI dimethylamine derivative **18** (30 mg, 0.06 mmol) in 2 ml of H_2O was added to azido-glyco-derivative (0.09 mmol, 1.5 eq.), dissolved into 2 ml of tBuOH. The suspension was stirrer at r.t. under nitrogen atmosphere for 2 h. The resulting red solution was concentrated under vacuum and a red solid was obtained. The crude product was analysed and purified by reverse phase column chromatography, (CH_3CN:H_2O 0.1%TFA) according to methods described in the previous section.

Compounds **1** and **2** (β-D-glc-*O*-C2-NDI-NMe_2 and α-D-man-*O*-C2-NDI-NMe_2) were synthesized according to the published synthetic protocol [21].

Compound **3**. β-D-gal-*O*-C2-NDI-NMe_2. Red solid, yield = 91%, ^{1}H NMR (300 MHz, D_2O), δ 8.21 (d, 1H, J_{orto} = 7.8 Hz), 8.13 (s, 1H); 7,97 (d, 1H, J_{orto} = 7.8 Hz), 7.88 (s, 1H), 4.79 (s, 1H), 4.63 (s, 2H), 4.25 (d, 1H, J = 7.9 Hz), 4.20 (m, 1H), 4.04 (bs, 4H), 3.74 (d, 1H, J = 3.3 Hz), 3.56–3.47 (m, 4H), 3.44 (d, 1H, J = 3.3 Hz), 3.33 (t, 1H, J = 7.9 Hz), 3.20–3.12 (m, 4H), 3.05 (d, 1H, J = 6.8 Hz), 2.82 (s, 12H), 2.05–2.03 (m, 4H). ^{13}C NMR (75 MHz, D_2O) δ 165.4; 163.9; 163.7; 163.3; 151.5; 143.5; 130.9; 128.3; 126.8; 124.7; 124.4; 122.3; 119.8; 118.5; 102.9; 99.4; 75.0; 72.4; 70.4; 68.3; 67.9; 60.7; 55.1; 50.4; 42.6; 37.8; 37.6; 36.9; 22.7. HRMS (ESI): m/z calculated for $C_{35}H_{46}N_8O_{10}$+H^+: 739.3410 $[M+H]^+$; found: 739.3409.

Compound **4**. β-D-malt-*O*-C2-NDI-NMe_2. Red solid, yield = 86%, ^{1}H NMR (300 MHz, D_2O), δ 8.18 (d, 1H, Jorto = 7.8 Hz), 8.12 (s, 1H); 7,94 (d, 1H, Jorto = 7.8 Hz), 7.80 (s, 1H), 4.77 (s, 2H), 4.61 (m, 2H), 4.20 (d, 1H, J = 8 Hz), 4.19–4.17 (m, 1H), 4.02 (m, 4H), 4.0–3.97 (m, 2H), 3.80 (d, 1H, J = 3.1 Hz), 3.66–3.62 (m, 3H), 3.50–3.45 (m, 3H), 3.36–3.23 (m, 3H), 3.22–3.14 (m, 4H), 3.11–2.91 (m, 2H), 2.83 (s, 12H), 2.08–2.0 (m, 4H). ^{13}C NMR (75 MHz, D_2O), δ 167.0; 165.4; 165.2; 164.7; 153.2; 132.8; 130.0; 128.4; 126.9; 126.4; 124.0; 121.5; 120.2; 119.9; 116.0; 104.8; 103.8; 101.1; 80.8; 77.1; 76.2; 75.8; 74.3; 74.2; 72.4; 70.1; 69.7; 62.6; 61.8; 57.0; 56.9; 52.2; 44.5; 44.4; 39.7; 39.5; 38.9; 24.6. HRMS (ESI): m/z calculated for $C_{41}H_{56}N_8O_{15}$+H^+: 901.3938 $[M+H]^+$; found: 901.3936.

Compound **9**. β-D-glc-*S*-C2-NDI-NMe_2. Red solid, Yield = 92%, ^{1}H NMR (300 MHz, D_2O), δ 8.12 (d, 1H, J_{orto} = 8 Hz), 8.09 (s, 1H); 7,88 (d, 1H, J_{orto} = 8 Hz), 7.72 (s, 1H), 4.76 (s, 1H), 4.61 (s, 2H), 4.23 (d, 1H, J = 9.7 Hz), 4.01 (bs, 4H), 3.69 (d, 1H, J = 12 Hz), 3.44 (dd, 1H, J = 6, 12 Hz), 3.24–3.18 (m, 8H), 3.06–3.00 (m, 2H), 2.99 (t, 1H, J = 9 Hz),

2.84 (s, 12H), 2.04 (m, 4H). ^{13}C NMR (75 MHz, D_2O), δ 165.1; 163.5; 163.3; 162.8; 151.3; 143.3; 130.9; 128.1; 126.4; 125.0; 124.9; 122.1; 119.8; 118.2; 114.2; 99.2; 85.2; 79.6; 76.9; 72.2; 69.3; 60.7; 55.1; 50.5; 42.7; 38.0; 37.6; 37.0; 22.7. HRMS (ESI): *m/z* calculated for $C_{35}H_{46}N_8O_{9S}$ + H^+: 755.3181 $[M+H]^+$; found: 755.3169.

Compound **10**. α-D-man-*S*-C2-NDI-NMe_2. Red solid, Yield = 92%, ^{1}H NMR (300 MHz, D_2O), δ 8.12 (s, 1H); 8.11 (d, 1H, J_{orto} = 8 Hz), 7,88 (d, 1H, J_{orto} = 8 Hz), 7.72 (s, 1H), 5.11 (s, 1H), 4.82 (s, 2H), 4.01 (t, 4H, *J* = 7 Hz), 3.78 (d, 1H, *J* = 2 Hz), 3.59−3.55 (m, 2H), 3.45 (t, 1H, *J* = 9 Hz), 3.34 (dd, 1H, *J* = 3, 8 Hz), 3.23−3.15 (m, 8H), 3.07 (m, 2H), 2.85 (s, 12H), 2.05 (m, 4H). ^{13}C NMR (75 MHz, D_2O) δ 165.2; 163.6; 163.3; 162.9; 151.3; 143.5; 130.9; 128.1; 126.5; 124.9; 124.6; 124.5; 122.2; 119.6; 118.2; 99.3; 85.0; 73.3; 71.4; 70.8; 66.6; 60.6; 55.2; 55.1; 49.7; 42.7; 38.0; 37.6; 37.0; 31.2; 22.7. HRMS (ESI): *m/z* calculated for $C_{35}H_{46}N_8O_9S$ + H^+: 755.3181 $[M+H]^+$; found: 755.3170.

Compound **11**. β-D-gal-*S*-C2-NDI-NMe_2. Red solid, yield = 89%, ^{1}H NMR (300 MHz, D_2O) δ 8.18 (d, *J* = 9.0 Hz, 1H), 8.11 (s, 1H), 7.94 (d, *J* = 9.0 Hz, 1H), 7.83 (d, *J* = 12Hz, 1H), 4.80 (s, 4H), 4.22 (d, *J* = 9.0 Hz, 1H), 4.04 (m, 4H), 3.77 (d, *J* = 3 Hz, 1H), 3.57−3.55 (m, 2H), 3.50−3.42 (m, 2H), 3.33−3.15 (m, 7H), 2.85 (s, 6H), 2.83 (s, 6H), 2.63 (s, 1H), 2.09−2.01 (m, 4H), 1.97 (s, 1H). ^{13}C NMR (75 MHz, D_2O) δ (ppm) = 164.9, 163.4, 163.2, 162.7, 151.1, 130.6, 127.8, 126.3, 124.7, 124.2, 121.9, 119.8; 118.07, 99.0, 85.3, 85.3, 78.5, 73.4, 69.1, 68.1, 60.6, 54.8, 54.8, 50.1, 42.3, 37.3, 36.6, 29.9, 22.3. HRMS (ESI): *m/z* calculated for $C_{35}H_{46}N_8O_9S$ + H^+: 755.3181 $[M+H]^+$; found: 755.3170.

Compound **12**. β-D-malt-*S*-C2-NDI-NMe_2. Red solid, yield = 74%, ^{1}H NMR (300 MHz, D_2O), δ 8.20 (d, 1H, J_{orto} = 8.0 Hz), 8.05 (s, 1H); 7.98 (d, 1H, J_{orto} = 8.0 Hz), 7.75 (s, 1H), 5.18 (s, 2H), 4.74 (s, 2H), 4.27 (d, 1H, *J* = 9.2 Hz), 3.89 (m, 4H), 3.66−3.35 (m, 12H), 3.18 (t, 1H, *J* = 9.2 Hz), 3.15 (bs, 4H), 3.11−2.98 (m, 2H), 2.77 (s, 12H), 1.93 (bs, 4H). ^{13}C NMR (75 MHz, D_2O), δ 165.3; 163.7; 163.5; 163.0; 151.5; 143.4; 131.1; 128.2, 127.3; 126.5; 125.2; 125.1; 124.7; 122.3; 120.0; 118.4; 99.8; 85.2; 78.1; 77.2; 77.1; 72.7; 72.6; 72.1; 71.5; 69.1; 60.6; 60.3; 55.2; 55.1; 50.3; 42.7; 38.1; 30.6; 22.7. HRMS (ESI): *m/z* calculated for $C_{41}H_{56}N_8O_{14}S$ + H^+: 917.3709 $[M+H]^+$; found: 917.3726.

Compound **17**. Prop-NDI-NMe_2 which was fully characterized according to the literature [21].

b) Carb-NDIs **5**−**8** and **13**−**16.** A solution of (+)-sodium-L-ascorbate (7.3 mg, 0.04 mmol), copper(II) sulfate pentahydrate (0.9 mg, 0.006 mmol) and alkynyl NDI morpholine derivative **19** (20 mg, 0.04 mmol) in 2 ml of H_2O was added to azido-glyco-derivative (0.06 mmol, 1.5 eq.), dissolved into 2 ml of tBuOH. The suspension was stirrer at r.t. under nitrogen atmosphere for 2 h. The resulting red solution was concentrated under vacuum and a red solid was obtained. The crude product was analysed and purified by reverse phase column chromatography, (CH_3CN:H_2O 0.1%TFA) according to methods described in the previous section.

Compound **5**. β-D-glc-*O*-C2-NDI-morph. Red solid, Yield = 81%, ^{1}H NMR (300 MHz, D_2O), δ 8.33 (d, J_{orto} = 7.9 Hz, 1H), 8.11 (d, J_{orto} = 6.43 Hz, 1H), 8.08 (s, 1H), 8.03 (s, 1H), 4.85 (s, 2H), 4.65−4.62 (m, 4H), 4.48−4.46 (m, 4H), 4.28 (d, *J* = 7.88 Hz, 1H), 4.06 (m, 6H), 3.74−3.69 (m, 10H), 3.51−3.46 (m, 6H), 3.30−3.22 (m, 6H), 3.03 (m, 2H), 1.26 (d, *J* = 6.68 Hz, 1H). ^{13}C NMR (75 MHz, D_2O), δ 165.5; 164.1; 164.03; 163.46; 151.73; 143.66; 131.22; 128.66; 126.89; 125.33; 124.75; 122.52; 120.28; 118.78; 102.23; 99.52; 75.71; 75.37; 72.84; 69.41; 67.81; 63.54; 60.48; 54.65; 54.32; 52.16; 50.39; 37.86; 34.66; 34.23. HRMS (ESI): *m/z* calculated for $C_{37}H_{46}N_8O_{12}$+H^+: 795.3308 $[M+H]^+$; found: 795.3292.

Compound **6**. α-D-man-*O*-C2-NDI-morph. Red solid, Yield = 72%, ^{1}H NMR (300 MHz, D_2O), δ 8.3 (d, J_{orto} = 7.83 Hz, 1H), 8.08 (s, 1H), 8.04 (d, J_{orto} = 9.48 Hz, 1H), 4.84 (s, 2H), 4.78 (s, 1H), 4.65 (m, 4H), 4.59 (m, 2H), 4.42−4.41 (m, 4H), 3.86 (m, 8H), 3.67 (m, 1H), 3.48−3.31 (m, 20H). ^{13}C NMR (75 MHz, D_2O), δ 165.53, 164.19, 163.55, 160.82, 151.84, 131.17, 131.11, 130.64, 129.05, 128.79, 124.65, 124.47, 122.57, 113.45, 103.47, 99.41, 72.61, 70.25, 69.75, 66.09, 63.75, 60.45, 60.40, 54.66, 54.29, 53.43, 53.38, 52.21, 50.07, 43.10, 37.79, 34.93, 33.85. HRMS (ESI): *m/z* calculated for $C_{37}H_{46}N_8O_{12}$+H^+: 795.3308 $[M+H]^+$; found: 795.3275.

Compound **7**. β-D-gal-*O*-C2-NDI-morph. Red solid, Yield = 25%, ^{1}H NMR (300 MHz, D_2O), δ 8.23 (d, J_{orto} = 7.9 Hz, 1H), 8.16 (s, 1H), 8.0 (d, J_{orto} = 7.85 Hz, 1H), 7.93 (s, 1H), 4.8 (s, 2H), 4.66−4.63 (m, 4H), 4.45−4.43 (m, 4H), 4.28−4.26 (m, 3H), 4.08−4.04 (m, 6H), 3.78−3.46 (m, 17H), 3.37 (m, 2H), 3.22 (m, 4H). ^{13}C NMR (75 MHz, D_2O), δ 165.23, 163.89, 163.73, 163.19, 151.53, 143.35, 131.14, 128.42, 126.64, 125.05, 124.84, 122.26, 120.14, 118.52, 102.92, 99.22, 74.99, 72.49, 70.47, 68.36, 67.90, 63.51, 60.76, 54.57, 54.28, 52.13, 50.45, 37.92, 34.64, 34.19. HRMS (ESI): *m/z* calculated for $C_{37}H_{46}N_8O_{12}$+H^+: 795.3308 $[M+H]^+$; found: 795.3281.

Compound **8**. β-D-malt-*O*-C2-NDI-morph. Red solid, Yield = 85%, ^{1}H NMR (300 MHz, D_2O), δ 8.3 (d, J_{orto} = 7.88 Hz, 1H), 8.08−8.05 (m, 2H), 7.95 (s, 1H), 5.02 (d, *J* = 3.59 Hz, 1H), 4.84 (s, 2H), 4.7−4.62 (m, 6H), 4.43−4.4 (m, 4H), 4.28 (d, *J* = 9.84 Hz, 2H), 3.88 (m, 8H), 3.68 (d, *J* = 10.1 Hz, 1H), 3.52−3.2 (m, 28H), 2.97 (m, 1H). ^{13}C NMR (75 MHz, D_2O), δ 165.44, 164.04, 163.96, 163.36, 151.75, 131.19, 128.61, 126.83, 125.32, 125.05, 124.73, 122.50, 120.42, 118.75, 99.72, 99.59, 85.14, 78.14, 77.15, 77.01, 72.68, 72.57, 72.06, 71.44, 69.08, 63.73, 63.68, 60.57, 60.31, 54.58, 54.23, 52.16, 50.30, 37.94, 34.84, 34.36. HRMS (ESI): *m/z* calculated for $C_{43}H_{56}N_8O_{17}$+H^+: 957.3836 $[M+H]^+$; found: 957.3805.

Compound **13**. β-D-glc-*S*-C2-NDI-morph. Red solid, Yield = 90% ^{1}H NMR (300 MHz, D_2O), δ 8.4 (d, J_{orto} = 7.9 Hz, 1H), 8.16 (d, J_{orto} = 7.9 Hz, 1H), 8.1 (m, 2H), 4.9 (s, 2H), 4.6 (m, 4H) 4.5−4.49 (m, 4H), 4.19 (d, *J* = 9.88 Hz, 1H), 4.07 (m, 4H), 3.7−3.69 (m, 10H), 3,47 (m, 6H), 3.28−3.12 (m, 10H), 3.02 (d, *J* = 9.19 Hz, 1H). ^{13}C NMR (75 MHz, D_2O), δ 168.72, 167.30, 166.69, 154.92, 134.25, 131.88, 130.07, 128.51, 127.87, 127.81, 125.73, 123.55, 122.03, 102.83, 88.10, 82.70, 79.91, 75.24, 72.24, 66.57, 63.68, 57.71, 57.33, 55.18, 53.53, 40.88, 37.65, 37.28, 33.14. HRMS (ESI): *m/z* calculated for $C_{37}H_{46}N_8O_{11}S$ + H^+: 811.3080 $[M+H]^+$; found: 811.3053.

Compound **14**. α-D-man-*S*-C2-NDI-morph. Red solid, Yield = 88%, ^{1}H NMR (300 MHz, D_2O), δ 8.21 (d, J_{orto} = 7.91 Hz, 1H), 8.13 (s, 1H), 7.98 (d, J_{orto} = 7.87 Hz, 1H), 7.88 (s, 1H), 5.12 (s, 1H), 4.79 (s, 2H), 4.66 (m, 2H), 4.44−4.42 (m, 5H), 4.08−4.04 (m, 5H), 3.85 (s, 1H), 3.73−3.58 (m, 12H), 3.52−3.47 (m, 7H), 3.24−3.11 (m, 7H) ^{13}C NMR (75 MHz, D_2O), δ 165.3, 163.9, 163.7, 163.2, 151.6, 143.5, 131.2, 128.4, 126.7, 125.1, 124.7, 124.6, 122.3, 120.1, 118.6, 99.3, 84.8, 73.2, 71.5, 70.9, 66.8, 63.6, 60.6, 54.6, 54.3, 52.2, 49.8, 38.0, 34.7, 34.2, 30.8. HRMS (ESI): *m/z* calculated for $C_{37}H_{46}N_8O_{11}S$ + H^+: 811.3080 $[M+H]^+$; found: 811.3049.

Compound **15**. β-D-gal-*S*-C2-NDI-morph. Red solid, Yield = 82%, ^{1}H NMR (300 MHz, D_2O), δ 8.3 (d, J_{orto} = 7.89 Hz, 1H), 8.13 (s, 1H), 8.07 (d, J_{orto} = 7.86 Hz, 1H), 7.99 (s, 1H), 4.85 (s, 2H), 4.7 (m, 4H), 4.46−4.44 (m, 4H), 4.24−4.21 (d, *J* = 9.47 Hz, 1H), 4.05 (m, 4H), 3.79−3.10 (m, 23H), 1.23 (m, 4H). ^{13}C NMR (75 MHz, D_2O), δ 168.48, 167.12, 167.01, 166.42, 154.75, 146.55, 134.19, 131.65, 129.86, 128.29, 127.73, 125.50, 123.38, 122.01, 121.79, 102.52, 88.71, 81.86, 76.73, 72.50, 71.51, 66.55, 63.92, 57.66, 57.28, 57.23, 55.16, 53.51, 45.41, 40.92, 37.64, 37.24, 33.19. HRMS (ESI): *m/z* calculated for $C_{37}H_{46}N_8O_{11}S$ + H^+: 811.3080 $[M+H]^+$; found: 811.3070.

Compound **16**. β-D-malt-*S*-C2-NDI-morph. Red solid, Yield = 70%. ^{1}H NMR (300 MHz, D_2O) δ 8.22 (d, *J* = 12 Hz, 1H), 8.03 (s, 1H), 7.98 (d, *J* = 8.0 Hz, 1H), 7.87 (s, 1H), 5.00 (d, *J* = 4.0 Hz, 1H), 4.76 (m, 2H), 4.57 (s, 2H), 4.38 (s, 4H), 4.24 (d, *J* = 10 Hz, 1H), 4.02−3.96 (m, 4H), 3.64−2.91 (m, 28H), 2.95 (t, *J* = 10 Hz, 2H). ^{13}C NMR (75 MHz, D2O) δ 165.5, 164.1, 164.0, 163.5, 151.8, 143.6, 131.3,

128.7, 126.9, 125.3, 125.0, 124.8, 122.6, 120.5, 118.8, 99.8, 99.6, 85.2, 78.2, 77.2, 77.1, 72.7, 72.6, 72.1, 71.5, 69.2, 63.6, 60.7, 60.4, 54.7, 54.3, 52.2, 50.4, 38.0, 34.7, 34.2, 30.4. HRMS (ESI): *m/z* calculated for $C_{43}H_{56}N_8O_{16}S + H^+$: 973.3608 $[M+H]^+$; found: 973.3588.

4.3. Biophysical methods

4.3.1. FRET melting assay

FRET melting assay was performed in 96-well plates and the fluorescence of the different labelled oligonucleotides was recorded using a CFX96 qPCR instrument (Biorad). Oligonucleotides were annealed at 0.23 μM strand concentration (95 °C, 5min) in K10 buffer (10 mM, 10 mM lithium cacodylate, 90 mM LiCl, pH 7.2). After a slow cool down to room temperature, they were added to each well (final concentration of 0.2 μM) which was incubated with or without the tested ligands, to a final volume of 25 μL. Competition experiments were performed in presence of a non-labelled auto complementary duplex, ds26, in 3 and 10 fold excess. The microplate was incubated at 25 °C for 5 min, after which the temperature was increased by increments of 0.5 °C per minute to reach 95 °C. The collected signal was normalized to 1 and the melting temperature (Tm) was defined when the normalized signal was 0.5. ΔTm corresponds to the difference of Tm between the oligonucleotides with and without the ligands. Ligands were tested in duplicates.

4.3.2. Mass spectrometry

The experiments were performed on a Bruker 7T SolariX XR ESI-Q-FTICRMS (Bruker, Bremen, Germany) with the ESI source operated in negative ion mode. The injection flow rate was 180 μL/h. All spectra were acquired in soft conditions [50]. The capillary exit voltage was −180 V, and skimmer 1 voltage was −5 V. The collision energy (entrance of the hexapole collision cell) was set to 1 V. Sample preparation: The stock solutions of the oligonucleotides (50 μM concentration) are prepared in 100 mM ammonium acetate (NH_4Ac). The mixture of ligand with DNA solution is made by dilution up to 5 μM in DNA and 10 μM in ligand.

4.4. Biological methods

4.4.1. Cell culture

'Single marker' (S16) BSF *T. brucei* (Lister 427, antigenic type MiTat 1.2, clone 221a) [51] were cultured at 37 °C, 5% CO2 in HMI-9 medium supplemented with 20% heat-inactivated fetal bovine serum (hiFBS, Invitrogen), as previously described [52]. *L. major* (MHOM/IL/80/Friedlin) promastigotes were cultured at 28 °C in modified RPMI-1640 medium (Invitrogen, Carlsbad, CA) [52]. HT-29 and MRC-5 cells were cultured in DMEM (Invitrogen) medium plus 10% hiFBS serum [10]. MRC-5 cells were grown in monolayer (5% CO_2, 37 °C) in DMEM medium (4.5 g/L glucose for HT-29 cells and 1 g/L for MRC-5), supplemented with 10% inactivated Fetal Bovine Serum, 100 U/mL penicillin, 100 mg/mL streptomycin and 2 mM L-glutamine. Cells were plated and passaged according to ATCC recommendations and were used for the experiments while in the exponential growth phase.

4.4.2. Antiparasitic activity

The trypanocidal activity of the compounds was assessed by the alamarBlue® assay (ThermoFisher scientific) [10,53]. Briefly, 1×10^3 BSF T. brucei were incubated in 96-wells plates alone or in the presence of increasing concentrations of compounds for 72 h (5% CO_2, 37 °C). 20 mL resazurin (110 ng/mL) were then added and the parasites were incubated for 4 additional hrs at 37 °C. Finally, cells were lysed with 50 mL of 3% SDS solution. Fluorescence was measured with an Infinite F200 plate reader (Tecan Austria, GmbH), exciting at 550 nm and recording the emission at 590 nm. The results are expressed as the concentration of compound that reduces cell growth by 50% versus untreated control cells (IC50) using SigmaPlot (Four Parameter Logistic Curve). Data are presented as the average of three independent measurements all conducted in triplicate conditions.

The leishmaniacidal activity of the compounds in experiments of drug susceptibility on L. major (MHOM/IL/80/Friedlin) was first carried out on promastigotes as previously described [51]. Briefly, 1×10^6/mL promastigotes were incubated for 72 h at 28 °C in 96-well plates in modified RPMI-1640 medium supplemented with 10% hiFBS, containing increasing concentration of compounds. Cell proliferation was determined using a MTT-based assay [54]. IC50 was calculated as described above.

4.4.3. Cytotoxicity

Cytotoxicity was measured through the MTT assay [55] as previously reported [10]. Briefly, 5×10^3 MRC-5 or HT-29 cells were seeded in 96-wells plates in the presence of increasing concentrations of compounds. After 48 h of incubation at 37 °C, 10 mL of MTT solution (5 mg/mL) were added to each well and cells were reincubated for 4h at 37 °C. The medium was then removed and DMSO was added. The plate was reincubated at 37 °C for 1 h and then analysed at the plate reader, measuring the absorption at 575 nm. IC50 was calculated as described above.

4.4.4. Cellular and parasitic uptake assays

225,000 cells (HT-29 or MRC5) were harvested by trypsinization and incubated with 10 μM of a NDI-Compound in 0.75 mL of medium for 2 h at 37 °C. After centrifugation (30 s at 13,000 rpm), supernatant removal (by pippeting), and washing with 1x PBS (3 times), the cell pellet was resuspended in 3% sodium dodecyl sulfate (SDS; 750 mL), sonicated (30 min) and homogenized by vortexing. Fluorescence values were then normalized through a protein quantification assay by using Pierce BCA tests (ThermoFisher Scientific) according to the manufacturer. Compound concentration values were extrapolated from a fluorescence−NDI concentration calibration curve carried out with cells lysates. Fluorescence was detected with a TECAN infinite F200 fluorescence-intensity multiplate reader (excitation wavelength: 485 nm, emission wavelength: 535 nm).

200,000 parasites (BSF T. brucei) were incubated with 7,89 μM of a NDI-Compound in 0.95 mL of medium for 2 h at 37 °C. After centrifugation (30 s at 13,000 rpm), supernatant removal (by Eppendorf inverting), and washing with 1X PBS (3 times), the cell pellet was resuspended in 10% sodium dodecyl sulfate (SDS; 300 mL), sonicated (30 min) and homogenized by vortexing. Fluorescence values were then normalized through a protein quantification assay by using Pierce BCA tests (ThermoFisher Scientific) according to the manufacturer. Compound concentration values were extrapolated from a fluorescence−NDI concentration calibration curve carried out with cells lysates. Fluorescence was detected with a TECAN infinite F200 fluorescence-intensity multiplate reader (excitation wavelength: 485 nm, emission wavelength: 535 nm).

4.4.5. Fluorescence microscopy

T. brucei parasites (1×10^7 / mL) were incubated with compounds **4** or **12** (5 μM), in 0.5 mL of medium without FBS for 30 and 120 min at 37 °C and 100% of humidity. The parasitic samples were then centrifuged, the supernatant was removed and parasites were fixed with 200 mL of cold paraformaldehyde 4% for 30 min on an ice bath. Then, samples were washed twice with 500mL cold phosphate buffered saline (PBS), the supernatant was removed and prolong DAPI staining (10mL) was added. 15 minutes later 3 mL of the sample was loaded to a poly lysine carrier and processed by

microscope observation. HT-29 cells (2×10^4 cells/mL) were growth (in 0.5 mL of medium without FBS) on a cover slide in a 24 well culture plate for 24h and then treated with compounds **4** or **12** (25 μM) for 30 or 120 min at 37 °C. After that, covers were washed 5 times (inside the wells) with 500mL room temperature PBS and fixed on an ice bath with paraformaldehyde 2% for 20 minutes. Two extra PBS washings (10 minutes each) were also necessary. Then, the cover slide was immersed first in water and lately in ethanol and let it to dry over a whattman paper. In the final step Prolong DAPI (3-4 mL) was used as mounting medium and samples were processed by microscope observation.Images were acquired using a widefield DMI8 LED microscope. Excitation was done with the 375-435 and 542-566 filters for DAPI and compounds **4** or **12**, respectively. A quadruple filter was used to detect the fluorescence emission of both, DAPI (437-474 nm) and compounds **4** or **12** (578-610 nm). Wide field images were adquired by DIC (differential interference contrast technique)The images were deconvoluted using Huygens Professional image processing software from Scientific Volume Imaging (http://www.svi.nl). The merge of the images was made with Fiji software (https://fiji.sc/).

Declaration of competing interest

The authors declare that they have no known competing financial interests or personal relationships that could have appeared to influence the work reported in this paper.

Acknowledgements

This work was funded by the Spanish Ministerio de Economía y Competitividad (RTI2018-099036-B-I00; EUIN2017-88791), Agence Nationale de la Recherche (ANR-20-CE12-0023, ANR-18-CE29-0013-POLYnESI) and INCa grants G4Access and A.B. was supported by an AIRC fellowship.

Appendix A. Supplementary data

Supplementary data to this article can be found online at https://doi.org/10.1016/j.ejmech.2022.114183.

References

[1] S.A. Ohnmacht, S. Neidle, Small-molecule quadruplex-targeted drug discovery, Bioorg. Med. Chem. Lett 24 (2014) 2602–2612, https://doi.org/10.1016/j.bmcl.2014.04.029.

[2] C.K. Kwok, C.J. Merrick, G-Quadruplexes, Prediction, characterization, and biological application, Trends Biotechnol. 35 (2017) 997–1013, https://doi.org/10.1016/j.tibtech.2017.06.012.

[3] S. Balasubramanian, L.H. Hurley, S. Neidle, Targeting G-quadruplexes in gene promoters: a novel anticancer strategy? Nat. Rev. Drug Discov. 10 (2011) 261–275. http://www.ncbi.nlm.nih.gov/entrez/query.fcgi?cmd=Retrieve&db=PubMed&dopt=Citation&list_uids=21455236.

[4] F.-Y. Teng, Z.-Z. Jiang, M. Guo, X.-Z. Tan, F. Chen, X.-G. Xi, Y. Xu, G-quadruplex DNA: a novel target for drug design, Cell. Mol. Life Sci. (2021), https://doi.org/10.1007/s00018-021-03921-8.

[5] J. Carvalho, J.-L. Mergny, G.F. Salgado, J.A. Queiroz, C. Cruz, G-quadruplex, friend or foe: the role of the G-quartet in anticancer strategies, Trends Mol. Med. 26 (2020) 848–861, https://doi.org/10.1016/j.molmed.2020.05.002.

[6] R. Simone, P. Fratta, S. Neidle, G.N. Parkinson, A.M. Isaacs, G-quadruplexes, Emerging roles in neurodegenerative diseases and the non-coding transcriptome, FEBS Lett. 589 (2015) 1653–1668, https://doi.org/10.1016/j.febslet.2015.05.003.

[7] S. Asamitsu, M. Takeuchi, S. Ikenoshita, Y. Imai, H. Kashiwagi, N. Shioda, Perspectives for applying G-quadruplex structures in neurobiology and neuropharmacology, Int. J. Mol. Sci. 20 (2019), https://doi.org/10.3390/ijms20122884.

[8] E. Ruggiero, S.N. Richter, Survey and summary G-quadruplexes and G-quadruplex ligands: targets and tools in antiviral therapy, Nucleic Acids Res. 46 (2018) 3270–3283, https://doi.org/10.1093/nar/gky187.

[9] H.L. M, M.K. R, N. Florian, F.M. Toyin, S. Nicolas, D. Christian, H. Paul, M.C. J, G-quadruplex DNA motifs in the malaria parasite plasmodium falciparum and their potential as novel antimalarial drug targets, Antimicrob. Agents Chemother. 62 (2021), https://doi.org/10.1128/AAC.01828-17 e01828-17.

[10] E. Belmonte-Reche, M. Martinez-Garcia, A. Guedin, M. Zuffo, M. Arevalo-Ruiz, F. Doria, J. Campos-Salinas, M. Maynadier, J.J. Lopez-Rubio, M. Freccero, J.L. Mergny, J.M. Perez-Victoria, J.C. Morales, G-quadruplex identification in the genome of Protozoan parasites points to naphthalene diimide ligands as new antiparasitic agents, J. Med. Chem. 61 (2018) 1231–1240, https://doi.org/10.1021/acs.jmedchem.7b01672.

[11] A.R. Duarte, E. Cadoni, A.S. Ressurreição, R. Moreira, A. Paulo, Design of modular G-quadruplex ligands, ChemMedChem 13 (2018) 869–893, https://doi.org/10.1002/cmdc.201700747.

[12] L. Savva, S.N. Georgiades, Recent developments in small-molecule ligands of medicinal relevance for harnessing the anticancer potential of G-quadruplexes, Mol 26 (2021), https://doi.org/10.3390/molecules26040841.

[13] S.A. Ohnmacht, C. Marchetti, M. Gunaratnam, R.J. Besser, S.M. Haider, G. Di Vita, H.L. Lowe, M. Mellinas-Gomez, S. Diocou, M. Robson, J. Sponer, B. Islam, R.B. Pedley, J.A. Hartley, S. Neidle, A G-quadruplex-binding compound showing anti-tumour activity in an in vivo model for pancreatic cancer, Sci. Rep. 5 (2015) 11385, https://doi.org/10.1038/srep11385.

[14] Z. Li, C. Liu, C. Huang, X. Meng, L. Zhang, J. He, J. Li, Quinazoline derivative QPB-15e stabilizes the c-myc promoter G-quadruplex and inhibits tumor growth in vivo, Oncotarget 7 (No 23) (2016) 34266–34276, 7, https://www.oncotarget.com/article/9088/text/.

[15] M.-H. Hu, T.-Y. Wu, Q. Huang, G. Jin, New substituted quinoxalines inhibit triple-negative breast cancer by specifically downregulating the c-MYC transcription, Nucleic Acids Res. 47 (2019) 10529–10542, https://doi.org/10.1093/nar/gkz835.

[16] D. Drygin, A. Siddiqui-Jain, S. O'Brien, M. Schwaebe, A. Lin, J. Bliesath, C.B. Ho, C. Proffitt, K. Trent, J.P. Whitten, J.K. Lim, D. Von Hoff, K. Anderes, W.G. Rice, Anticancer activity of CX-3543: a direct inhibitor of rRNA biogenesis, Cancer Res. 69 (2009) 7653–7661, https://doi.org/10.1158/0008-5472.CAN-09-1304.

[17] A. Local, H. Zhang, K. Benbatoul, P. Folger, S. Sheng, C.-Y. Tsai, S. Howell, W. Rice, APTO-253 interaction with G-quadruplex DNA is linked to inhibition of c-myc expression, induction of DNA damage, and generation of synthetic lethality in cells with BRCA1/2 impairment, Blood 130 (2017) 5094, https://doi.org/10.1182/blood.V130.Suppl_1.5094.5094.

[18] A. Local, H. Zhang, K.D. Benbatoul, P. Folger, X. Sheng, C.-Y. Tsai, S.B. Howell, W.G. Rice, APTO-253 stabilizes G-quadruplex DNA, inhibits MYC expression, and induces DNA damage in acute myeloid leukemia cells, Mol. Cancer Therapeut. 17 (2018) 1177, https://doi.org/10.1158/1535-7163.MCT-17-1209. LP – 1186.

[19] H. Xu, M. Di Antonio, S. McKinney, V. Mathew, B. Ho, N.J. O'Neil, N. Dos Santos, J. Silvester, V. Wei, J. Garcia, F. Kabeer, D. Lai, P. Soriano, J. Banáth, D.S. Chiu, D. Yap, D.D. Le, F.B. Ye, A. Zhang, K. Thu, J. Soong, S. Lin, A.H.C. Tsai, T. Osako, T. Algara, D.N. Saunders, J. Wong, J. Xian, M.B. Bally, J.D. Brenton, G.W. Brown, S.P. Shah, D. Cescon, T.W. Mak, C. Caldas, P.C. Stirling, P. Hieter, S. Balasubramanian, S. Aparicio, CX-5461 is a DNA G-quadruplex stabilizer with selective lethality in BRCA1/2 deficient tumours, Nat. Commun. 8 (2017) 14432, https://doi.org/10.1038/ncomms14432.

[20] C.W. Schultz, G.A. McCarthy, T. Nerwal, A. Nevler, J.B. DuHadaway, M.D. McCoy, W. Jiang, S.Z. Brown, A. Goetz, A. Jain, V.S. Calvert, V. Vishwakarma, D. Wang, R. Preet, J. Cassel, R. Summer, H. Shaghaghi, Y. Pommier, S.A. Baechler, M.J. Pishvaian, T. Golan, C.J. Yeo, E.F. Petricoin, G.C. Prendergast, J. Salvino, P.K. Singh, D.A. Dixon, J.R. Brody, The FDA-approved anthelmintic pyrvinium pamoate inhibits pancreatic cancer cells in nutrient-depleted conditions by targeting the mitochondria, Mol. Cancer Therapeut. (2021), https://doi.org/10.1158/1535-7163.MCT-20-0652.

[21] M. Arevalo-Ruiz, F. Doria, E. Belmonte-Reche, A. De Rache, J. Campos-Salinas, R. Lucas, E. Falomir, M. Carda, J.M. Perez-Victoria, J.L. Mergny, M. Freccero, J.C. Morales, Synthesis, binding properties, and differences in cell uptake of G-quadruplex ligands based on carbohydrate naphthalene diimide conjugates, Chem. Eur J. 23 (2017) 2157–2164, https://doi.org/10.1002/chem.201604886.

[22] M. Zuffo, A. Stucchi, J. Campos-Salinas, M. Cabello-Donayre, M. Martínez-García, E. Belmonte-Reche, J.M. Pérez-Victoria, J.L. Mergny, M. Freccero, J.C. Morales, F. Doria, Carbohydrate-naphthalene diimide conjugates as potential antiparasitic drugs: synthesis, evaluation and structure-activity studies, Eur. J. Med. Chem. 163 (2019) 54–66, https://doi.org/10.1016/j.ejmech.2018.11.043.

[23] E.C. Calvaresi, P.J. Hergenrother, Glucose conjugation for the specific targeting and treatment of cancer, Chem. Sci. 4 (2013) 2319–2333, https://doi.org/10.1039/C3SC22205E.

[24] H. Li, X. Gao, R. Liu, Y. Wang, M. Zhang, Z. Fu, Y. Mi, Y. Wang, Z. Yao, Q. Gao, Glucose conjugated platinum(II) complex: antitumor superiority to oxaliplatin, combination effect and mechanism of action, Eur. J. Med. Chem. 101 (2015) 400–408, https://doi.org/10.1016/j.ejmech.2015.07.006.

[25] M. Patra, T.C. Johnstone, K. Suntharalingam, S.J. Lippard, A potent glucose-platinum conjugate exploits glucose transporters and preferentially accumulates in cancer cells, Angew Chem. Int. Ed. Engl. 55 (2016) 2550–2554, https://doi.org/10.1002/anie.201510551.

[26] H. Song, S.J. Allison, V. Brabec, H.E. Bridgewater, J. Kasparkova, H. Kostrhunova, V. Novohradsky, R.M. Phillips, J. Pracharova, N.J. Rogers, S.L. Shepherd, P. Scott, Glycoconjugated metallohelices have improved nuclear delivery and suppress tumour growth in vivo, Angew. Chem. Int. Ed. 59 (2020) 14677–14685, https://doi.org/10.1002/anie.202006814.

[27] X. Zhao, P. Zhang, Y. Li, S. Wu, F. Li, Y. Wang, S. Liang, X. He, Y. Zeng, Z. Liu,

Glucose−lipopeptide conjugates reveal the role of glucose modification position in complexation and the potential of malignant melanoma therapy, J. Med. Chem. 64 (2021) 11483−11495, https://doi.org/10.1021/acs.jmedchem.1c00805.
[28] J.C. Morales, Synthesis of carbohydrate-oligonucleotide conjugates and their applications, in: M.J.C.-R.J. Fernández-Lucas (Ed.), Enzym. Chem. Synth. Nucleic Acid Deriv., WILEY-VCH Verlag, Weinheim, 2019, pp. 259−290.
[29] Q.-L. He, I. Minn, Q. Wang, P. Xu, S.A. Head, E. Datan, B. Yu, M.G. Pomper, J.O. Liu, Targeted delivery and sustained antitumor activity of triptolide through glucose conjugation, Angew. Chem. Int. Ed. 55 (2016) 12035−12039, https://doi.org/10.1002/anie.201606121.
[30] V. Sanchez-Martin, D.A. Schneider, M. Ortiz-Gonzalez, A. Soriano-Lerma, A. Linde-Rodriguez, V. Perez-Carrasco, J. Gutierrez-Fernandez, M. Cuadros, J.C. Morales, C. González, M. Soriano, J.A. García-Salcedo, Targeting ribosomal G-quadruplexes with naphthalene-diimides as RNA polymerase I inhibitors for colorectal cancer treatment, Cell Chem. Biol. 28 (2021) 1591−1601, https://doi.org/10.1016/j.chembiol.2021.05.021.
[31] H. Driguez, in: H. Driguez, J. Thiem (Eds.), Thiooligosaccharides in Glycobiology BT - Glycoscience Synthesis of Substrate Analogs and Mimetics, Springer Berlin Heidelberg, Berlin, Heidelberg, 1998, pp. 85−116, https://doi.org/10.1007/BFb0119254.
[32] C.A. De Leon, P.M. Levine, T.W. Craven, M.R. Pratt, The sulfur-linked analogue of O-GlcNAc (S-GlcNAc) is an enzymatically stable and reasonable structural surrogate for O-GlcNAc at the peptide and protein levels, Biochemistry 56 (2017) 3507−3517, https://doi.org/10.1021/acs.biochem.7b00268.
[33] G. Siciliano, M. Corricelli, R.M. Iacobazzi, F. Canepa, D. Comegna, E. Fanizza, A. Del Gatto, M. Saviano, V. Laquintana, R. Comparelli, G. Mascolo, S. Murgolo, M. Striccoli, A. Agostiano, N. Denora, L. Zaccaro, M.L. Curri, N. Depalo, Gold-speckled SPION@SiO2 nanoparticles decorated with thiocarbohydrates for ASGPR1 targeting: towards HCC dual mode imaging potential applications, Chem. Eur J. 26 (2020) 11048−11059, https://doi.org/10.1002/chem.202002142.
[34] D. Comegna, I. de Paola, M. Saviano, A. Del Gatto, L. Zaccaro, Straightforward entry to S-glycosylated fmoc-amino acids and their application to solid phase synthesis of glycopeptides and glycopeptidomimetics, Org. Lett. 17 (2015) 640−643, https://doi.org/10.1021/ol503664t.
[35] M. Gingras, Y.M. Chabre, M. Roy, R. Roy, How do multivalent glycodendrimers benefit from sulfur chemistry? Chem. Soc. Rev. 42 (2013) 4823−4841, https://doi.org/10.1039/C3CS60090D.
[36] J.M. Madeira, D.L. Gibson, W.F. Kean, A. Klegeris, The biological activity of auranofin: implications for novel treatment of diseases, Inflammopharmacology 20 (2012) 297−306, https://doi.org/10.1007/s10787-012-0149-1.
[37] E. Jortzik, M. Farhadi, R. Ahmadi, K. Tóth, J. Lohr, B.M. Helmke, S. Kehr, A. Unterberg, I. Ott, R. Gust, V. Deborde, E. Davioud-Charvet, R. Réau, K. Becker, C. Herold-Mende, Antiglioma activity of GoPI-sugar, a novel gold(I)−phosphole inhibitor: chemical synthesis, mechanistic studies, and effectiveness in vivo, Biochim. Biophys. Acta Protein Proteon. 1844 (2014) 1415−1426, https://doi.org/10.1016/j.bbapap.2014.01.006.
[38] M. Micco, G.W. Collie, A.G. Dale, S.A. Ohnmacht, I. Pazitna, M. Gunaratnam, A.P. Reszka, S. Neidle, Structure-based design and evaluation of naphthalene diimide G-quadruplex ligands as telomere targeting agents in pancreatic cancer cells, J. Med. Chem. 56 (2013) 2959−2974, https://doi.org/10.1021/jm301899y.
[39] V. Yarlagadda, M.M. Konai, G.B. Manjunath, C. Ghosh, J. Haldar, Tackling vancomycin-resistant bacteria with 'lipophilic−vancomycin−carbohydrate conjugates, J. Antibiot. 68 (2015) 302−312, https://doi.org/10.1038/ja.2014.144.
[40] S. Park, I. Shin, Carbohydrate microarrays for assaying galactosyltransferase activity, Org. Lett. 9 (2007) 1675−1678, https://doi.org/10.1021/ol070250l.
[41] J. Morales-Sanfrutos, J. Lopez-Jaramillo, M. Ortega-Muñoz, A. Megia-Fernandez, F. Perez-Balderas, F. Hernandez-Mateo, F. Santoyo-Gonzalez, Vinyl sulfone: a versatile function for simple bioconjugation and immobilization, Org. Biomol. Chem. 8 (2010) 667−675, https://doi.org/10.1039/B920576D.
[42] E. Belmonte-Reche, M. Martinez-Garcia, P. Penalver, V. Gomez-Perez, R. Lucas, F. Gamarro, J.M. Perez-Victoria, J.C. Morales, Tyrosol and hydroxytyrosol derivatives as antitrypanosomal and antileishmanial agents, Eur. J. Med. Chem. 119 (2016) 132−140, https://doi.org/10.1016/j.ejmech.2016.04.047.
[43] A.M. Zheoat, S. Alenezi, E.K. Elmahallawy, M.A. Ungogo, A.H. Alghamdi, D.G. Watson, J.O. Igoli, A.I. Gray, H.P. de Koning, V.A. Ferro, Antitrypanosomal and antileishmanial activity of chalcones and flavanones from polygonum salicifolium, Pathogens 10 (2021) 179−186, https://doi.org/10.3390/pathogens10020175.
[44] A. De Cian, L. Guittat, M. Kaiser, B. Sacca, S. Amrane, A. Bourdoncle, P. Alberti, M.P. Teulade-Fichou, L. Lacroix, J.L. Mergny, Fluorescence-based melting assays for studying quadruplex ligands, Methods 42 (2007) 183−195, https://doi.org/10.1016/j.ymeth.2006.10.004.
[45] V. Gabelica, S. Livet, F. Rosu, Optimizing native ion mobility Q-TOF in helium and nitrogen for very fragile noncovalent structures, J. Am. Soc. Mass Spectrom. 29 (2018) 2189−2198, https://doi.org/10.1007/s13361-018-2029-4.
[46] H.R. Drew, R.M. Wing, T. Takano, C. Broka, S. Tanaka, K. Itakura, R.E. Dickerson, Structure of a B-DNA dodecamer: conformation and dynamics, Proc. Natl. Acad. Sci. Unit. States Am. 78 (1981) 2179, https://doi.org/10.1073/pnas.78.4.2179. LP − 2183.
[47] F. Rosu, E. De Pauw, V. Gabelica, Electrospray mass spectrometry to study drug-nucleic acids interactions, Biochimie 90 (2008) 1074−1087, https://doi.org/10.1016/j.biochi.2008.01.005.
[48] V. Gabelica, F. Rosu, E. De Pauw, A simple method to determine electrospray response factors of noncovalent complexes, Anal. Chem. 81 (2009) 6708−6715, https://doi.org/10.1021/ac900785m.
[49] J.-X. Wang, Q. Chen, N. Bian, F. Yang, J. Sun, A.-D. Qi, C.-G. Yan, B.-H. Han, Sugar-bearing tetraphenylethylene: novel fluorescent probe for studies of carbohydrate−protein interaction based on aggregation-induced emission, Org. Biomol. Chem. 9 (2011) 2219−2226, https://doi.org/10.1039/C0OB00680G.
[50] F. Balthasart, J. Plavec, V. Gabelica, Ammonium ion binding to DNA G-quadruplexes: do electrospray mass spectra faithfully reflect the solution-phase species? J. Am. Soc. Mass Spectrom. 24 (2013) 1−8, https://doi.org/10.1007/s13361-012-0499-3.
[51] E. Wirtz, S. Leal, C. Ochatt, G.M. Cross, A tightly regulated inducible expression system for conditional gene knock-outs and dominant-negative genetics in Trypanosoma brucei, Mol. Biochem. Parasitol. 99 (1999) 89−101, https://doi.org/10.1016/S0166-6851(99)00002-X.
[52] M. Cabello-Donayre, S. Malagarie-Cazenave, J. Campos-Salinas, F.J. Gálvez, A. Rodríguez-Martínez, E. Pineda-Molina, L.M. Orrego, M. Martínez-García, M.P. Sánchez-Cañete, A.M. Estévez, J.M. Pérez-Victoria, Trypanosomatid parasites rescue heme from endocytosed hemoglobin through lysosomal HRG transporters, Mol. Microbiol. 101 (2016) 895−908, https://doi.org/10.1111/mmi.13430.
[53] E.M. Larson, D.J. Doughman, D.S. Gregerson, W.F. Obritsch, A new, simple, nonradioactive, nontoxic in vitro assay to monitor corneal endothelial cell viability, Invest. Ophthalmol. Vis. Sci. 38 (1997) 1929−1933.
[54] J.M. Perez-Victoria, B.I. Bavchvarov, I.R. Torrecillas, M. Martinez-Garcia, C. Lopez-Martin, M. Campillo, S. Castanys, F. Gamarro, Sitamaquine overcomes ABC-mediated resistance to miltefosine and antimony in Leishmania, Antimicrob. Agents Chemother. 55 (2011) 3838−3844, https://doi.org/10.1128/AAC.00065-11.
[55] T. Mosmann, Rapid colorimetric assay for cellular growth and survival: application to proliferation and cytotoxicity assays, J. Immunol. Methods 65 (1983) 55−63. http://www.ncbi.nlm.nih.gov/pubmed/6606682.